Effect of initial conditions on a one-dimensional model of small-amplitude wave propagation in shallow water. II: Blowup for nonsmooth conditions

J.I. Ramos and Carmen María García López

Escuela de Ingenierías Industriales, Universidad de Málaga, Málaga, Spain

Abstract

Purpose – The purpose of this paper is to analyze numerically the blowup in finite time of the solutions to a one-dimensional, bidirectional, nonlinear wave model equation for the propagation of small-amplitude waves in shallow water, as a function of the relaxation time, linear and nonlinear drift, power of the nonlinear advection flux, viscosity coefficient, viscous attenuation, and amplitude, smoothness and width of three types of initial conditions.

Design/methodology/approach – An implicit, first-order accurate in time, finite difference method valid for semipositive relaxation times has been used to solve the equation in a truncated domain for three different initial conditions, a first-order time derivative initially equal to zero and several constant wave speeds.

Findings – The numerical experiments show a very rapid transient from the initial conditions to the formation of a leading propagating wave, whose duration depends strongly on the shape, amplitude and width of the initial data as well as on the coefficients of the bidirectional equation. The blowup times for the triangular conditions have been found to be larger than those for the Gaussian ones, and the latter are larger than those for rectangular conditions, thus indicating that the blowup time decreases as the smoothness of the initial conditions decreases. The blowup time has also been found to decrease as the relaxation time, degree of nonlinearity, linear drift coefficient and amplitude of the initial conditions are increased, and as the width of the initial condition is decreased, but it increases as the viscosity coefficient is increased. No blowup has been observed for relaxation times smaller than one-hundredth, viscosity coefficients larger than ten-thousandths, quadratic and cubic nonlinearities, and initial Gaussian, triangular and rectangular conditions of unity amplitude.

Originality/value – The blowup of a one-dimensional, bidirectional equation that is a model for the propagation of waves in shallow water, longitudinal displacement in homogeneous viscoelastic bars, nerve conduction, nonlinear acoustics and heat transfer in very small devices and/or at very high transfer rates has been determined numerically as a function of the linear and nonlinear drift coefficients, power of the nonlinear drift, viscosity coefficient, viscous attenuation, and amplitude, smoothness and width of the initial conditions for nonzero relaxation times.

1. Introduction

Most models developed to date for the study of wave propagation in shallow water, such as,
for example, the Korteweg–de Vries (Korteweg and de Vries, 1895) and Benjamin–Bona–
Mahony (BBM) or regularized long-wave (RLW) equations and modifications and
generalizations thereof (Peregrine, 1966, 1967; Benjamin *et al.*, 1972; Ramos, 2016; Ramos
and García López, 2017; Johnson, 1997; Lannes, 2013; Debnath, 1994; Dingemans, 1997),
have been obtained by means of asymptotic methods, Taylor's series expansions, depth-
averaging techniques (Whitham, 1974; Ramos, 2016; Ramos and García López, 2017), etc.,
and are one-dimensional and unidirectional, i.e. waves propagate only in one direction.

One-dimensional, bidirectional models of wave propagation in shallow water include
Wu's long-wave model (Wu, 1994) and the two-equation Boussinesq model for the wave
height and flow speed (Boussinesq, 1871, 1872), the good (McKean, 1981) and bad (Yang and
Wang, 2003) Boussinesq equations and modifications thereof (Bona *et al.*, 2002, 2004;
Dutykh and Dias, 2007; Dutykh, 2009; Carter, 2018). It must be noted that one-dimensional
Boussinesq models include fourth-order spatial derivatives, e.g. the (linearly stable) good
Boussinesq equation:

$$u_{tt} = u_{xx} - u_{xxxx} + (u^2)_{xx},$$

which does not include viscous damping. Other Boussinesq models for surface water waves
include viscosity (Le Meur, 2015).

Bona *et al.* (2002) derived a four-parameter family of Boussinesq equations for small
amplitude long waves as approximations to the two-dimensional Euler's equations for
inviscid fluids, studied their linear stability, well-posedness and energy conservation and
argued that linear well-posedness is a natural requirement for the possible physical
relevance of model equations. In a subsequent publication, Bona *et al.* (2004) showed that
first-order correct models that are linearly well-posed are locally nonlinearly well-posed
and that, in some cases, global well-posedness is established for physical relevant initial
data.

An open problem in fluid dynamics is whether or not the three-dimensional Euler
equations develop singularities in finite time; in addition, there is as yet no proof that
solutions to the Navier–Stokes equations exist and whether or not they are unique. These
problems are part of the Millennium Prize Problems proposed by The Clay Mathematics
Institute of Cambridge, Massachusetts, in 2000.

For the three-dimensional Euler equations, finite-time blowup for nonsmooth initial
conditions has been proven mathematically by Elgindi (2021), but the question of blowup in
finite time for smooth initial conditions is still unresolved. Finite-time blowup for the time-
dependent, axisymmetric Euler equations in cylindrical coordinates has also been reported
in some numerical experiments (Luo and Hou, 2014, 2019) that show a dramatic growth in
the maximum magnitude of the vorticity and suggest the formation of a singularity. Finite-
time blowup has also been observed in other wave propagation problems (Yordanov and
Zhang, 2005; Caffarelli and Friedman, 1986) and nonlinear reaction–diffusion equations, e.g.
Pierre and Schmitt (2000).

In this paper, blowup of the following one-dimensional nonlinear model equation for bidirectional wave propagation in shallow water:

$$\tau u_{tt} + u_t + \alpha u_x + \epsilon(u^p)_x = \mu u_{xx} + \delta u_{xxt}, \tag{1}$$

is numerically studied for $\tau \neq 0$, $\mu \neq 0$, and three different initial conditions, where $u(t, x)$ is the wave amplitude, t and x denote the time and spatial coordinate, respectively, τ can be interpreted as a relaxation or characteristic memory time, μ is the viscosity coefficient, δ is the viscous attenuation (hereon, also referred to as dispersion) coefficient, α is the linear drift/advection coefficient, and ϵ and $p \neq 1$ stand for the coefficient and power of the nonlinear drift, respectively. Note that, for $\delta = 0$, $\tau \neq 0$ and $\mu \neq 0$, equation (1) is a second-order, semi-linear, hyperbolic equation with two characteristic lines of slope equal to $\pm\sqrt{\frac{\mu}{\tau}}$. For $\delta = 0$, $\tau = 0$ and $\mu \neq 0$, equation (1) is a parabolic equation characterized by an infinite speed of propagation. On the other hand, for $\delta \neq 0$, $\tau \neq 0$ and $\mu \neq 0$, equation (1) may be written as $\tau v_t + v u_t + \alpha u_x + \epsilon(u^p)x = \mu u_{xx} + \delta v_{xx}$, which indicates that the dynamics of $v(t, x)$ depends on a linear friction term, i.e. v, and a viscous one, i.e. v_{xx}, where $v \equiv u_t$.

Equation (1) includes a large variety of equations of interest in engineering and science, e.g. the one-dimensional heat and mass diffusion equations, the linear, first-order wave equation, the second-order hyperbolic equation, the standard, modified and generalized, inviscid and viscous Burgers, the standard, modified and generalized, inviscid and viscous equal-width equations (Onder *et al.*, 2023; Ramos, 2006, 2007), etc. Moreover, as shown in Part I (Ramos and García López, 2020), equation (1) reduces to that of the standard ($p = 2$), modified ($p = 3$) and generalized ($p > 3$) inviscid RLW equations when both the relaxation time and the viscosity coefficient are nil. The standard (Saka *et al.*, 2011; Mittal and Rohila, 2018), modified (Karakoç *et al.*, 2013, 2014, 2015) and generalized (Ramos, 2016; García López and Ramos, 2015; Ramos and García López, 2017; Karakoç and Zeybek, 2016; Zeybek and Karakoç, 2019; Karakoç *et al.*, 2022) inviscid RLW equations, as well as the standard, modified and generalized inviscid equal-width (Onder *et al.*, 2023) equations have been the subject of a large number of numerical studies aimed at understanding solitary wave propagation and interactions between solitary waves and assessing the accuracy of numerical methods by comparing the numerical results with the available analytical solutions for these equations and their finite number of invariants. By way of contrast, few analytical and numerical studies on the viscous equal-width (Ramos, 2006, 2007) and viscous RLW equations (García López and Ramos, 2015) which may be obtained from equation (1) by setting $\tau = 0$, have been reported. This is not surprising because while the inviscid RLW equation has solitary wave solutions characterized by a constant wave speed that depends on the wave amplitude, the solutions to the viscous RLW equations exhibit damping, do not have constant wave speeds and exhibit curved trajectories (García López and Ramos, 2015).

The dynamics of equation (1) have been previously studied for $\tau \neq 0$, $\mu \neq 0$, $u_t(0, x) = 0$ and initial conditions corresponding to the solution of the inviscid generalized RLW equation as well as initial conditions of the Gaussian type (Ramos and García López, 2020); the initial conditions considered in Part I are infinitely differentiable and were found to result in steep propagating fronts and, in some cases, weak blowup. Note that the dispersion term in equation (1) is analogous to that of the inviscid generalized RLW equation and contains second-order spatial derivatives but not fourth-order ones (compare with the good Boussinesq equation above).

Equation (1) can also be written as $\tau u_{tt} + u_t - \delta u_{xxt} = (\mathcal{F}(u, u_x))_x$, where $\mathcal{F}(u, u_x) = -\alpha u - \epsilon u^p + \mu u_x$, which is similar to that which appears in models of passive and active,

i.e. "smart," vibration devices constructed from polymer composites, i.e. elastomers filled with carbon black and/or silica or with active elements (Banks *et al.*, 1997), the longitudinal displacement in homogeneous viscoelastic bars of uniform cross section (Zhijian and Changming, 1997), and the deformation of viscoelastic materials of the rate type (Yang and Wang, 2003). As indicated in Part I, equation (1) also includes some of the model equations used in nonlinear acoustics in viscous and heat-conducting media with relaxation and absorption, impulsive motions of viscoelastic fluids, dynamics of second-order fluids, low-frequency seismic effects on fluid-saturated reservoirs, etc. (Ramos and García López, 2020.)

A one-dimensional equation analogous to equation (1) but without the linear and nonlinear first-order spatial derivative terms has also been used to model nerve conduction (Rinzel and Keller, 1973; Keener and Sneyd, 2009) and heat transfer processes in very small devices and/or at very high rates (Joseph and Preziosi, 1989, 1990). A generalization of equation (1) in two dimensions which does not include the linear and nonlinear advection terms has also been studied numerically by means of the differential quadrature method by Mittal and Dahiya (2018).

Depending on the initial conditions and parameters that appear in equation (1), its Cauchy initial-value problem may exhibit blowup in finite time, even if it is linearly well-posed. Furthermore, the first term in the left-hand side of equation (1) may be interpreted as a memory or relaxation term, and its introduction results in a second-order hyperbolic operator, which together with the nonlinearity appearing in that equation, may result in a blowup phenomenon analogous to that observed in the hyperbolic Burgers equation (Escudero, 2007), which may be obtained from equation (1) for $\alpha = 1$, $\delta = 0$, $p = 2$ and $\epsilon = \frac{1}{2}$.

It must be pointed out that the hyperbolic Burgers equation used by Escudero (2007) cannot be obtained from the well-known viscous Burgers equation (Burgers, 1948) with a delayed stress because a first-order Taylor's series expansion approximation of the stress results in a Maxwell–Cattaneo model (Jou *et al.*, 1985; Joseph and Preziosi, 1989, 1990) that includes further nonlinearities associated with the time-derivative of the first-order hyperbolic operator that appears in Burgers equation. However, the hyperbolic Burgers equation analyzed by Escudero (2007) may be interpreted as a model of phenomena exhibiting relaxation and/or memory (Khonkin, 1980; Khonkin and Orlov, 1993; Rosenau, 1993).

The paper has been arranged as follows. In Section 2, ordinary differential equations for the mass and potential energy of the solution to equation (1) are derived as functions of the stretching and kinetic energies and the parameters that appear in that equation and the initial conditions; these equations differ from and are much simpler than those presented in Part I (Ramos and García López, 2020) where the reader may also find the analytical solution to equation (1). In Section 2, the three types of initial conditions considered here with $u_t(0, x) = 0$, i.e. for constant mass, are reported, and the potential and stretching energies are determined. Two of the initial conditions are continuous; the one corresponding to a Gaussian distribution is continuously differentiable, whereas that of triangular conditions is piecewise smooth. The third type of initial conditions is also piecewise smooth but has not classical first-order spatial derivatives at the locations of the vertical sides of the rectangle. These three conditions contain the same mass and are used to determine the effects of their amplitude, smoothness and width on the wave dynamics and blowup in finite time. The numerical method used in this study is the same as that used in Part I to determine the wave dynamics of equation (1) in the absence of blowup and is summarized in Section 2. In Section 3, the results of some numerical experiments on blowup with homogeneous Dirichlet boundary

conditions are reported for the three initial conditions considered in this paper, and several values of the relaxation time, viscosity coefficient, linear drift velocity and the coefficient and power of the nonlinear advection term. A final section summarizes the main findings of the paper.

2. Formulation

For $\delta = 0$, and $\tau \neq 0$ and $\mu \neq 0$, equation (1) is a second-order, quasilinear, hyperbolic equation characterized by two characteristic lines along which the velocity is $c = \pm\sqrt{\frac{\mu}{\tau}}$. In addition, equation (1) contains a linear advection coefficient, α, and δ has dimensions of length squared that defines a dispersion time equal to $\frac{\sqrt{\delta}}{\alpha}$. By analogy with aerodynamics, the conditions $|\alpha| > |c|$ and $|\alpha| < |c|$ correspond to supersonic and subsonic propagation, respectively.

Equation (1) is also characterized by the relaxation time τ and a diffusion–dispersion time equal to $\frac{\delta}{\mu}$ which results from the balance between the diffusion and dispersion terms in that equation. Therefore, the dynamics of equation (1) depends on three time scales, i.e. τ, $\frac{\delta}{\mu}$ and $\frac{\sqrt{\delta}}{\alpha}$, a length scale equal to $\sqrt{\delta}$, and any other length scale introduced by the initial conditions.

Although equation (1) may be interpreted as a dimensionless model equation for one-dimensional, bidirectional, nonlinear wave propagation in nonlinear (for $\epsilon \neq 0$ and $p > 1$) dissipative and dispersive media with memory/relaxation, it is possible, upon introducing L, T and U as characteristic time, length and velocity scales, respectively, to write that equation as:

$$\tau u_{tt} + u_t + u_x + (u^p)_x = \mu u_{xx} + u_{xxt}, \tag{2}$$

upon scaling $u \to \frac{u}{U}$, $x \to \frac{x}{L}$ and $t \to \frac{t}{T}$, where, for the sake of convenience, the same symbols have been used for both the dimensional and the dimensionless variables, $U = \left(\frac{\alpha}{\epsilon}\right)^{\frac{1}{p-1}}$, $L = \sqrt{\delta}$ and $T = \frac{\sqrt{\delta}}{\alpha}$. This scaling is only valid for $\alpha \neq 0$; if this condition is not met, one may use $U = \sqrt{\frac{\mu}{\tau}}$, $L = \sqrt{\delta}$ and $T = \sqrt{\frac{\delta}{\mu}}$. Other scalings are also possible.

Even though equation (2) depends on fewer parameters than equation (1), in this paper, we shall be concerned with equation (1), so that we can illustrate the dynamics of that equation as a function of τ, α, p and μ for $\epsilon = \delta = 1$, and the three different types of smooth and nonsmooth initial conditions discussed in Section 2.3.

As indicated in Part I, equation (1) has a solitary wave solution of the inverse hyperbolic cosine type [cf. equation (3) of Part I] analogous to those of the RLW and modified and generalized RLW equations, if $c = \alpha + 2\frac{\epsilon}{p+1}A^{p-1} = \pm\sqrt{\frac{\mu}{\tau}}$, where A and c denote the solitary wave's amplitude and speed, respectively, for $p \neq 1$. This implies that this inverse hyperbolic cosine solution is only physically valid for $\sqrt{\frac{\mu}{\tau}} > \alpha$, i.e. supersonic conditions, and that the wave speed only depends on the ratio of the viscosity coefficient to the relaxation time, whereas, for the inviscid RLW and modified and generalized, inviscid RLW equations, i.e. equation (1) with $\mu = \tau = 0$, the wave speed depends on α, p, δ, ϵ and the wave's amplitude.

2.1 Mass conservation
As shown in Part I, the spatial integration of equation (1) subject to $u(t, \pm\infty) = u_x(t, \pm\infty) = 0$ yields:

$$\tau \frac{d^2 M}{dt^2}(t) + \frac{dM}{dt}(t) = 0, \tag{3}$$

whose solution is as follows:

$$M(t) \equiv \int_{-\infty}^{\infty} u(t,x)dx = \int_{-\infty}^{\infty} \left(u(0,x) + \tau \left(1 - \exp\left(-\frac{t}{\tau} \right) \right) u_t(0,x) \right) dx \tag{4}$$

where $M(t)$ will be hereon referred to as the mass.

Equation (4) indicates that the mass evolves from an initial value $M(0) = \int_{-\infty}^{\infty} u(0,x)dx$ to $M(\infty) = \int_{-\infty}^{\infty} (u(0,x) + \tau u_t(0,x))dx$, and, therefore, mass is not conserved unless $\tau = 0$, $u_t(0, x) = 0$ or $\int_{-\infty}^{\infty} u_t(0,x)dx$. Equation (4) also indicates that $M(t)$ increases with time if $\int_{-\infty}^{\infty} u_t(0,x)dx > 0$ and $\tau \neq 0$.

2.2 Energy conservation

In Part I, a rather long formulation was presented to determine the evolution of the potential energy associated with equation (1). Such a formulation was found very useful to analyze the wave dynamics in the absence of blowup as shown in Figures 3, 6, 10 and 13 of Part I. In this paper, a much simpler formulation which may also be obtained from equations (6) to (10) of Part I after lengthy algebra is reported.

Multiplication of equation (1) by $u(t, x)$ and integration of the resulting equation subject to the same boundary conditions as above, i.e. $u(t, \pm\infty) = u_x(t, \pm\infty) = 0$, yields the following:

$$\begin{aligned} E(t) = E(0) + \tau \left[\frac{dE}{dt}(0) + \frac{\delta}{\tau} D(0) \right] \left(1 - \exp\left(-\frac{t}{\tau} \right) \right) \\ - \frac{\delta}{\tau} \int_0^t D(s)ds + \tau \int_0^t (R(s) - \beta D(s)) \left(1 - \exp\left(-\frac{t-s}{\tau} \right) \right) ds \end{aligned} \tag{5}$$

where

$$E(t) = \int_{-\infty}^{\infty} u^2(t,x)dx, \quad D(t) = \int_{-\infty}^{\infty} (u_x)^2(t,x)dx, \quad R(t) = 2\int_{-\infty}^{\infty} (u_t)^2(t,x)dx, \tag{6}$$

will be hereon referred to as twice the potential energy, twice the stretching energy and four times the kinetic energy, respectively, $\beta = \frac{1}{\tau} - \frac{2\mu}{\delta}$, and $\tau \neq 0$. The finiteness of E, D and R demands that u, u_x and u_t be L_2-integrable in space for all times.

For $\tau = 0$, equation (5) becomes:

$$E(t) = E(0) + \delta(D(0) - D(t)) - 2\mu \int_0^t D(s)ds, \tag{7}$$

which indicates that the potential energy depends on the viscosity coefficient μ and the dispersion parameter δ. Equation (7) indicates that the potential energy decreases with time owing to both dispersion and dissipation and that, for $\mu = 0$, $E(t) + \delta D(t) = E(0) + \delta D(0)$, i.e. the sum of the potential and stretching energies is conserved. On the other hand, equation (5) shows that the potential energy depends on the relaxation time, τ, $\frac{\delta}{\tau}$ and $\frac{\mu\tau}{\delta}$ (or β).

Notice that the last term on the right-hand side of equation (5) is positive and makes a positive contribution to the potential energy for $\beta < 0$. The condition $\beta \leq 0$ implies that $2\frac{\mu\tau}{\delta} \geq 1$, i.e. $c^2 = \frac{\mu}{\tau} \geq \frac{\delta}{2\tau^2}$, which cannot be satisfied for a specified value of c (or specified values of $\frac{\mu}{\tau}$) as τ is decreased. Moreover, because, for $\tau = 0$, equation (1) becomes the viscous generalized RLW or BBM equation, the condition $0 < \tau \ll 1$ results in a singularly perturbed initial-boundary value problem that exhibits an initial layer for $\delta = O(1)$ (Kevorkian and Cole, 1981, 1996; Butuzov, 1997), as indicated in Part I, where further details on initial, boundary and corner layers for $0 < \tau \ll 1$ and/or $0 < \mu \ll 1$ are provided.

Equation (5) indicates that the potential energy decreases on account of the viscous dissipation represented by the third term in the right-hand side of that equation; it also shows that the potential energy may increase with time if $\frac{dE}{dt}(0) + \frac{\delta}{\tau}D(0) > 0$ [cf. the second term of the right-hand side of equation (5)], but such an increase is, at most, $\tau\left(\frac{dE}{dt}(0) + \frac{\delta}{\tau}D(0)\right)$. Equation (5) also shows that the potential energy increases, provided that the fourth term in its right-hand side is positive; therefore, if this term is positive and its magnitude is larger than the third one in the right-hand side of equation (5), then the potential energy increases with time and blowup in finite time may occur even when $\frac{dE}{dt}(0)$ is negative.

It is worth mentioning that the linear advection or drift coefficient α does not affect the potential energy in equation (5) due to the homogeneous Dirichlet boundary conditions for u considered in this paper; however, as it will be shown later, it will affect the blowup time.

Equation (5) may also be written as:

$$
\begin{aligned}
E(t) + \int_0^t D(s)\left[\frac{\delta}{\tau} + \tau\beta\left(1 - \exp\left(-\frac{t-s}{\tau}\right)\right)\right]ds = E(0)+ \\
+\tau\left[\frac{dE}{dt}(0) + \frac{\delta}{\tau}D(0)\right]\left(1 - \exp\left(-\frac{t}{\tau}\right)\right) + \tau\int_0^t R(s)\left(1 - \exp\left(-\frac{t-s}{\tau}\right)\right)ds,
\end{aligned}
\tag{8}
$$

which indicates that, for $\delta \geq 0$ and $\beta \geq 0$, the left-hand side of this equation increases with time from $E(0)$. The last term on the right-hand side of equation (8) has lower and upper bounds equal to 0 and $\tau\int_0^\infty R(s)ds \geq 0$, respectively.

In Part I, a linear temporal stability analysis of the linearized version of equation (1) was performed for real wavenumbers and complex frequencies, and it was found that the linearized equation is (Fourier's) linearly stable provided that c^2 is greater than or equal to $\frac{\alpha^2}{(1+\delta k^2)^2}$, where k is the wavenumber, and linearly unstable, otherwise. Because the smallest value of k is 0, the above linear stability condition implies that $c^2 \geq \alpha^2$. However, such a condition is based on a linear analysis which is strictly applicable to very small amplitudes and infinite spatial domains, i.e. (linear) Cauchy's initial-value problems, and does not account for nonlinear effects; neither does it account for boundary effects.

When $|u(t, x)|$ is large, the nonlinear advection term associated with $\epsilon \neq 0$ and $p \neq 1$ in equation (1) results in wave steepening for $u_x < 0$ and $\epsilon > 0$ that would lead to the formation of a (discontinuous) shock wave for $\tau = \mu = \delta = 0$, and the formation of a Taylor's (smooth) shock wave for $\tau = \delta = 0$ and $\mu > 0$ (Whitham, 1974; Johnson, 1997; Lannes, 2013; Debnath, 1994; Dingemans, 1997)). In the absence of linear drift and for $p = 2$, $\epsilon = \frac{1}{2}$ and $\delta = 0$, i.e. the hyperbolic Burgers equation, it has been proved that equation (1) exhibits blowup in finite time (Escudero, 2007).

2.3 Initial conditions

The effects of three different initial conditions on both the wave dynamics and the blowup of equation (1) have been studied for $u(t, \pm\infty) = u_x(t, \pm\infty) = 0$ and $u_t(x, 0) = 0$, i.e. $M(t) = M(0)$ [cf. equation (4)]. Similar conditions were used in Part I which dealt with the dynamics of equation (1) in the absence of blowup. In this section, the smoothness and main properties of these initial conditions are determined analytically.

The first initial condition considered in this study corresponds to the following Gaussian distribution:

$$u(0, x) = A\exp\left(-\sigma(x - x_0)^2\right), \tag{9}$$

where A, x_0 and σ are constants, A is here referred to as the amplitude of the initial conditions, x_0 denotes the location of the maximum value of $u(0, x)$ and $\frac{1}{\sqrt{\sigma}}$ provides an indication of the width of the Gaussian initial conditions. For these initial conditions, neither the generalized RLW equation nor equation (1) has an analytical solution.

From the Gaussian condition of equation (9), it can be easily deduced that:

$$M(0) = A\sqrt{\frac{\pi}{\sigma}}, \quad E(0) = A^2\sqrt{\frac{\pi}{2\sigma}} = \frac{1}{\sqrt{2}}AM(0),$$
$$D(0) = A^2\sqrt{\frac{\pi\sigma}{2}} = \frac{\pi}{\sqrt{2}}\frac{A^3}{M(0)}, \quad R(0) = 0, \tag{10}$$

which indicates that the initial mass and the potential and stretching energies increase with A; the initial mass and the potential energy decrease, whereas the stretching energy increases as σ is increased.

The second type of initial conditions considered in this study is of triangular type, i.e. $u(x, 0) = 0$ for $-\infty < x \leq x_0 - b$ and $x_0 + b \leq x < \infty$, $u(0, x) = \frac{A}{b}[x - (x_0 - b)]$ for $x_0 - b \leq x \leq x_0$, and $u(0, x) = \frac{A}{b}[x_0 + b - x]$ for $x_0 \leq x \leq x_0 + b$, where the area of the triangle is equal to $M(0)$ and its height is equal to A, i.e. $b = \frac{M(0)}{A}$. These initial conditions are characterized by the same amplitude and mass as those of the Gaussian conditions considered above and are not differentiable at x_0 and $x_0 \pm b$, although left- and right-side derivatives exist and are finite at these three locations.

For these triangular conditions, it is an easy exercise to show that:

$$M(0) = Ab, \quad E(0) = \frac{2}{3}A^2 b = \frac{2}{3}AM(0),$$
$$D(0) = 2\frac{A^2}{b} = 2\frac{A^3}{M(0)}, \quad R(0) = 0, \tag{11}$$

The largest values of $|u_x(0, x)|$ for the Gaussian and triangular conditions discussed above are $\sqrt{\frac{2\pi}{e}}\frac{A^2}{M(0)} \approx 1.52\frac{A^2}{M(0)}$ and $\frac{A^2}{M(0)}$, respectively.

The third type of initial conditions considered here are of the rectangular type, i.e. $u(0, x) = 0$ for $-\infty < x < x_0 - B$ and $x_0 + B < x < \infty$, $u(0, x) = A$ for $x_0 - B < x < x_0 + B$, where the area of the rectangle is equal to $M(0)$ and its height is equal to A, i.e. $B = \frac{M(0)}{2A}$. These initial conditions are characterized by the same amplitude and mass as those of the Gaussian and triangular conditions described above, and result in:

$$M(0) = 2AB, \quad E(0) = 2A^2B = AM(0), \quad R(0) = 0, \quad (12)$$

and $u_x(0, \pm B)$ is Dirac's (generalized) delta function.

2.4 Numerical method
The same time-linearized implicit finite difference method presented in Part I was used to obtain the numerical solution of equation (1) subject to the initial conditions described in the previous section. The infinite spatial domain was truncated into the finite one $[0, L]$, where $L = 150$, and x_0 was selected so that the locations of the left and right boundaries do not affect the wave dynamics and blowup.

In the numerical experiments reported in this paper, $x_0 = 20$, unless stated otherwise. Hereon, we shall refer to the left and right boundaries as upstream and downstream, respectively. In the cases that the waves collide with either the upstream or the downstream boundary, only results for times less than the collision time and not affected by the boundaries are presented.

The finite difference method used in this study is first-order accurate in time and second-order accurate in space and uses a second-order time linearization for the nonlinear terms, so that a linear system of algebraic equations at each time level results. This system is characterized by a tridiagonal matrix and was solved by means of the well-known Thomas algorithm. Further details on the numerical method and its implementation can be found in Part I, where the reader may also find a discussion on the assessment of its accuracy.

In the numerical experiments reported in this paper, homogeneous Dirichlet boundary conditions for $u(t, x)$ were specified at the edges of the computational domain, i.e. at $x = 0$ and $L = 150$; these boundary conditions are strictly applicable when the waves are sufficiently far away from the boundaries.

3. Presentation of results
In this section, the results of some numerical experiments that illustrate blowup for the three initial conditions discussed in the previous section are presented. For the sake of convenience, the effects of each parameter that appears in equation (1) on blowup has been assessed by using a time step and a grid spacing equal to 10^{-4} and 0.1, respectively, unless stated otherwise; this time step is at least ten times smaller than the smallest relaxation time used in the calculations reported in this section, and, therefore, there are about ten time intervals in the initial layer thickness for the smallest relaxation time considered in this study (Kevorkian and Cole, 1981, 1996; Butuzov, 1997). It should be noticed that many other numerical experiments that do not result in blowup have also been performed, but they are not reported here. Notice also that, as stated previously, $\epsilon = \delta = 1$, unless otherwise stated, and that, for the time step and grid size used in the numerical experiments reported here, the temporal discretization errors are about two orders of magnitude smaller than the spatial ones.

It should also be emphasized that only results that are not affected by the presence of the boundaries are reported here, although the calculations were performed for up to $t = 50$ even if the waves collided with the boundaries but the solution did not blow up.

The blowup time, i.e. t_{bu}, has been defined as that corresponding to $u(t_{bu}, x) \geq 5A$ for any $x \in [0, L]$. A much more accurate calculation of the blowup time requires both adaptive meshes in space and very short variable time steps to accurately resolve the steep gradients associated with the growth and/or singularity of $u(t, x)$. Notice that $\lim_{t \to t_{bu}} \max|u(t, x)| = \infty$. By using the blowup time criterion mentioned above, no such temporal and spatial

refinement are required, because the largest value of $|u(t_{bu}, x)|$ has been set to only five times the largest value of $|u(0, t)|$.

3.1 Results for Gaussian initial conditions
For Gaussian initial conditions, $A = 1$, $\sigma = 0.05$, $p = 2$, $\alpha = 1$, $\tau = 0.1$ and $c^2 = 0.1$, Figure 1 shows a smooth leading wave front propagating toward the downstream boundary; the amplitude of the leading wave increases with time and the wave exhibits a curved trajectory, thus indicating that its velocity is not constant. Figure 1 also shows that behind the leading wave front, i.e. between the leading wave and the upstream boundary, there are also small waves whose amplitude decreases as the distance from the leading wave increases or as the distance to the upstream boundary decreases; these oscillations are a consequence of the fact that the initial conditions considered in this study do not correspond to the exact solution of equation (1) (cf. Part I).

It should be noted that, for $\sigma = 0.05$ and 0.1, the number of grid points in the interval $\left[x_0 - \frac{1}{\sqrt{\sigma}}, x_0 + \frac{1}{\sqrt{\sigma}} \right]$ is about 89 and 59, respectively, and, therefore, the grid spacing used in the calculations presented in this section is sufficiently small to determine accurately the initial transition as well as the wave dynamics resulting from the initial Gaussian conditions.

As shown in Part I and Section 2, the exact solution of equation (1) requires that $c = \alpha + 2\frac{\epsilon}{p+1}A^{p-1}$ be equal to $c = \pm\sqrt{\frac{\mu}{\tau}}$ and is of the hyperbolic cosine type; neither of these two conditions are satisfied for the set of parameters of Figure 1.

The initial growth of the leading wave amplitude and the negative values of u observed in Figure 1 are in accord with the fact that $M(t) = M(0)$, i.e. mass is conserved.

Similar trends to those shown in Figure 1 have also been observed for the same parameters as those of that figure and $c^2 = 1$; however, in this case, the blowup time increases, i.e. it takes longer for the solution to blowup. This is a consequence of the fact that, for the same value of τ, an increase of c results in an increase of the viscosity coefficient.
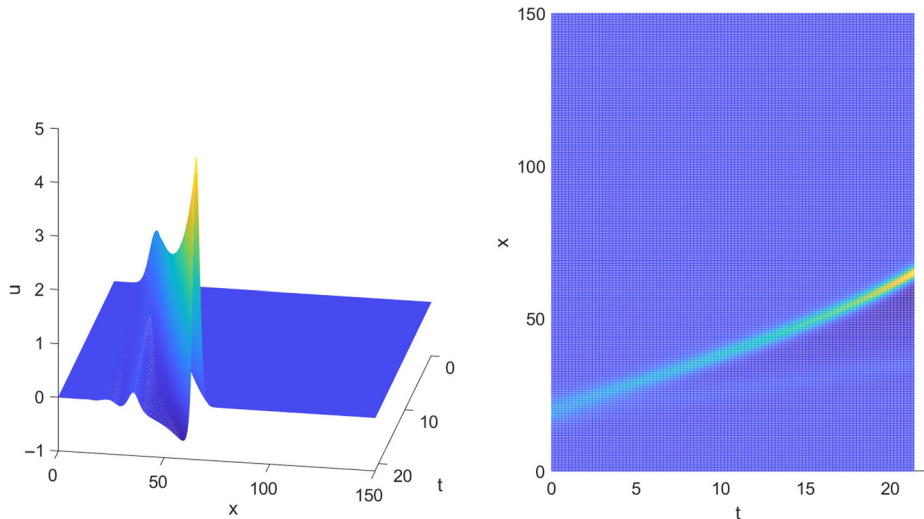

Figure 1.
$u(t, x)$ (left) and isocontours of $u(t, x)$ (right) for Gaussian initial conditions: $A = 1$, $\sigma = 0.05$, $\alpha = 1$, $c^2 = 0.1$, $\tau = 0.1$ and $p = 2$

Source: Figure by authors

For Gaussian initial conditions, $A = 1$, $\sigma = 0.05$, $p = 2$, $\alpha = 1$, $\tau = 0.01$ and $c^2 = 0.1$, Figure 2 indicates that the leading wave front propagates at a nearly constant speed and that no blowup occurs for $t \leq 50$. The background of this figure clearly shows the initial transient behavior from the Gaussian initial conditions used in this study to the formation of the leading wave front, as well as the waves/oscillations behind the leading wave front. The amplitude of these oscillations decreases as the distance to the upstream boundary decreases.

For the same values of the parameters as in Figure 2 except that $p = 3$ and $\tau = 0.1$, Figure 3 illustrates that the leading wave amplitude increases quite rapidly with time and that the amplitude of the oscillations behind the leading wave is of much larger amplitude than those observed in Figure 2, thus indicating that the blowup time decreases as the exponent of the nonlinear advection term in equation (1), p, is increased. Notice that equations (6) and (8) show that the potential energy increases as the kinetic energy increases, whereas it decreases as the stretching energy is increased.

For the same parameters as those of Figure 3 except that $\tau = 0.01$, analogous trends to those of Figure 3 have been observed except that no blowup occurs for $t \leq 50$, the leading wave amplitude increases at a small rate, the location of the leading wave maximum exhibits a convex trajectory with time and the number of oscillations behind the leading wave front shows similar trends to, but is larger than that of Figure 2.

Figure 4 shows the numerical solutions obtained for Gaussian initial conditions, $A = 1.5$, $\sigma = 0.05$, $p = 3$, $\alpha = 1$, $\tau = 0.01$ and $c^2 = 0.1$, and illustrates that the wave amplitude increases quite rapidly with time, the first wave behind the leading one propagates at an almost constant speed toward the downstream boundary, blowup occurs at about $t = 19$ and the distance between the leading wave and the next one behind it increases as time is increased, i.e. the leading wave trajectory is curved and its curvature decreases as time increases.

The results presented in Figure 4 exhibit blowup at $t \approx 19$. By way of contrast, for the same parameters as those of Figure 4 except that $\tau = 0.1$, blowup was observed at $t \approx 3.07$. As stated previously, for the same value of $c^2 = \frac{\mu}{\tau}$, an increase of τ, i.e. an increase of inertia or relaxation time, corresponds to an increase of μ, i.e. an increase of viscosity. Such as
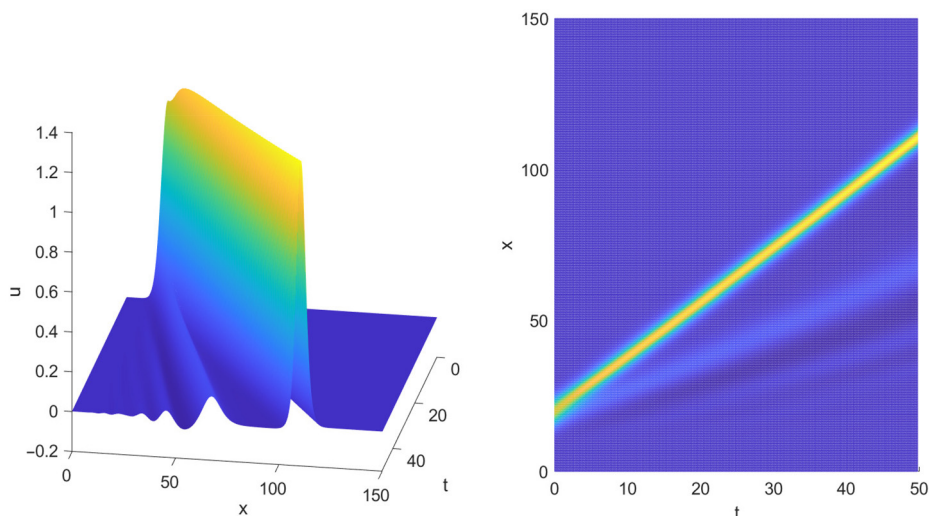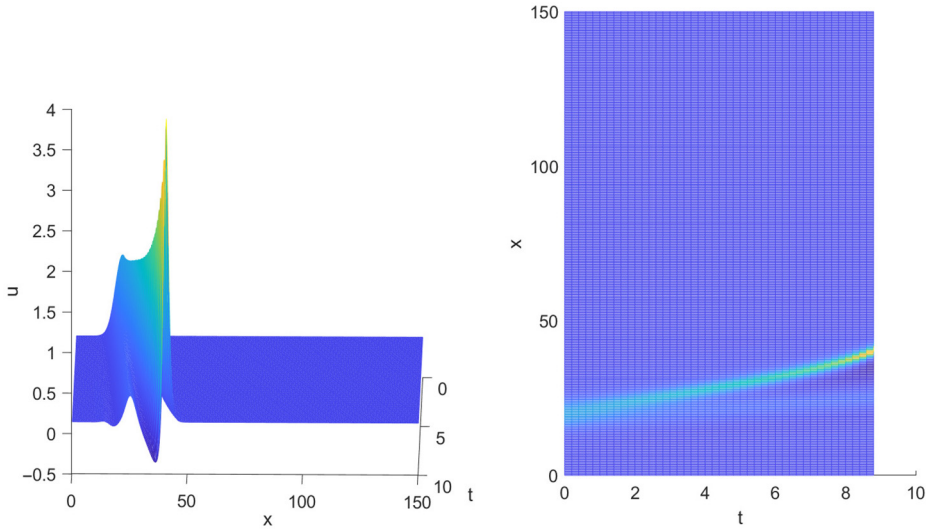

Source: Figure by authors

Figure 2. $u(t, x)$ (left) and isocontours of $u(t, x)$ (right) for Gaussian initial conditions: $A = 1$, $\sigma = 0.05$, $\alpha = 1$, $c^2 = 0.1$, $\tau = 0.01$ and $p = 2$
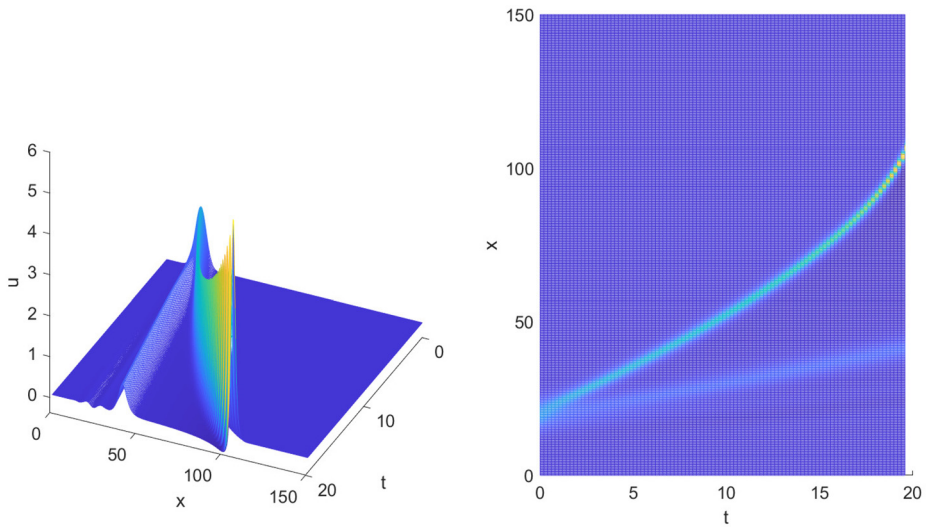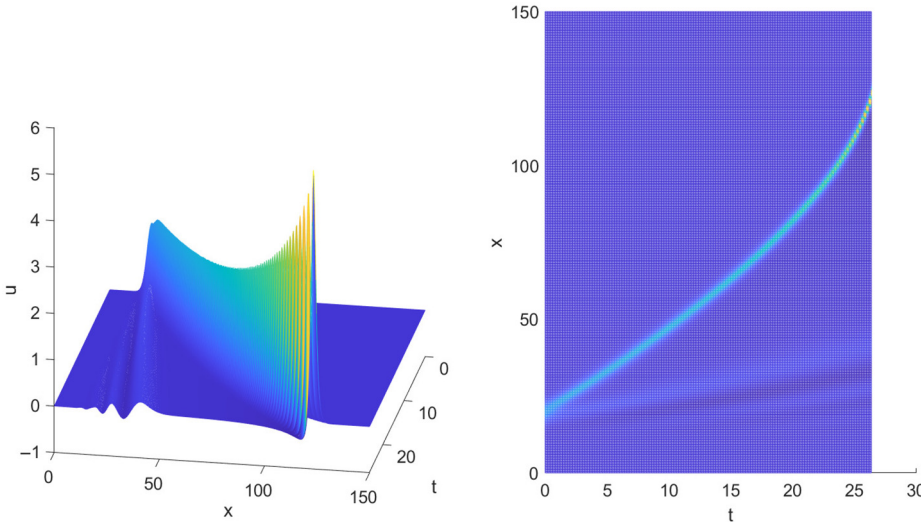
Blowup for nonsmooth conditions

1199

Source: Figure by authors

Source: Figure by authors

increase in μ may result in a negative value of β and, therefore, an increase of $E(t)$ [cf. equation (8)].

For the same conditions as those of Figure 4 except that $\sigma = 0.1$, the results presented in Figure 5 show that the blowup time increases as σ is increased; the curvature of the leading wave trajectory also increases as σ is increased, and the amplitude of the first wave behind

Source: Figure by authors

the leading one has a smaller amplitude than that of Figure 4. Notice that, as indicated previously, an increase of σ corresponds to a decrease of the width of the initial Gaussian condition, and, therefore, an increase of $u_x(0, t)$, i.e. an increase of the initial stretching energy which in accord with equations (6) and (8), results in an initial decrease of the potential energy, $E(t)$.

Figure 6 illustrates the results of numerical experiments performed for the same values of the parameters as those of Figure 4, except that $\alpha = 0.1$, i.e. for a linear drift speed ten times smaller than that of Figure 4. The results shown in Figure 6 exhibit similar trends to those presented in Figure 4, except that the blowup time for $\alpha = 0.1$ is larger than that for $\alpha = 1$; in addition, for $\alpha = 0.1$, $u(t, x)$ exhibits oscillations with a smaller number of negative values and larger positive amplitudes behind the leading wave front than for $\alpha = 1$.

Although not easily observed in Figures 4 and 6, the leading wave propagates at higher speed and exhibits a larger curvature for $\alpha = 1$ than for $\alpha = 0.1$, in accord with the characteristic lines of the first-order partial differential operator of equation (1), for $\mu = \delta = \tau = 0$ (Whitham, 1974; Johnson, 1997; Lannes, 2013; Debnath, 1994; Dingemans, 1997).

3.2 Results for triangular initial conditions

In this section, the results shown in Figures 7–12 correspond to triangular initial conditions and the same parameters as those of Figures 1–6, respectively, for Gaussian conditions. As indicated in equation (6) and discussed previously, it should be kept in mind that the triangular conditions have the same mass as the Gaussian ones. Moreover, for $\sigma = 0.05$ and 0.1, the number of grid points in the interval $[x_0 - b, x_0 + b]$, i.e. the base of the triangle, is about 111 and 157, respectively, and, therefore, the grid spacing used in the calculations presented in this section is sufficiently small to determine accurately the initial transition as well as the wave dynamics resulting from the triangular initial conditions considered in this study.
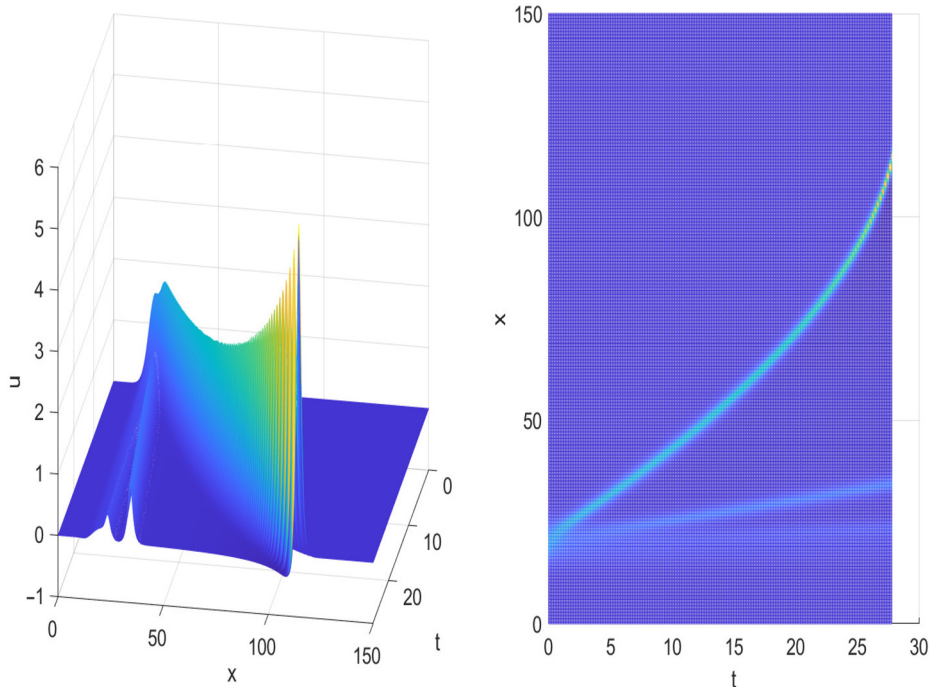
Figure 6.
$u(t, x)$ (left) and
isocontours of $u(t, x)$
(right) for Gaussian
initial conditions: $A =$
1.5, $\sigma = 0.05$, $\alpha = 0.1$,
$c^2 = 0.1$, $\tau = 0.01$ and
$p = 3$

Source: Figure by authors

Figure 7 corresponds to the same set of parameters as those of Figure 1 and shows a larger number of oscillations behind the leading wave and a slightly larger blowup time than Figure 1. The larger number of oscillations behind the leading wave is a consequence of the fact that the triangular initial conditions are not differentiable at the vertices of the triangle. Note that max $|u_x(0, x)|$ is larger for Gaussian conditions than for triangular ones; therefore, according to equation (6), the initial stretching energy of the Gaussian conditions is larger than that of the triangular ones.

Analogous results to those shown in Figure 7 have also been obtained for $c^2 = 1$, except that, in this case, the blowup time is larger and the amplitude of the oscillations behind the leading wave is smaller than those illustrated in Figure 7.

The wave dynamics presented in Figure 8 exhibits similar trends between the leading wave and the upstream boundary to those presented in Figure 2; however, the number of oscillations behind the leading wave is larger and closer to the upstream boundary than that of Figure 2.

Notice that, as indicated in Section 2.3 [cf. equations (10) and (11)], the initial potential and stretching energies associated with the triangular initial conditions are about 94% and 90%, respectively, of those of the Gaussian conditions, respectively, i.e. for the same initial mass, the triangular conditions have less initial potential and stretching energies than Gaussian ones.

Figure 9 corresponds to the same parameters as those of Figure 3 and shows that the blowup time corresponding to triangular initial conditions is larger than that for Gaussian
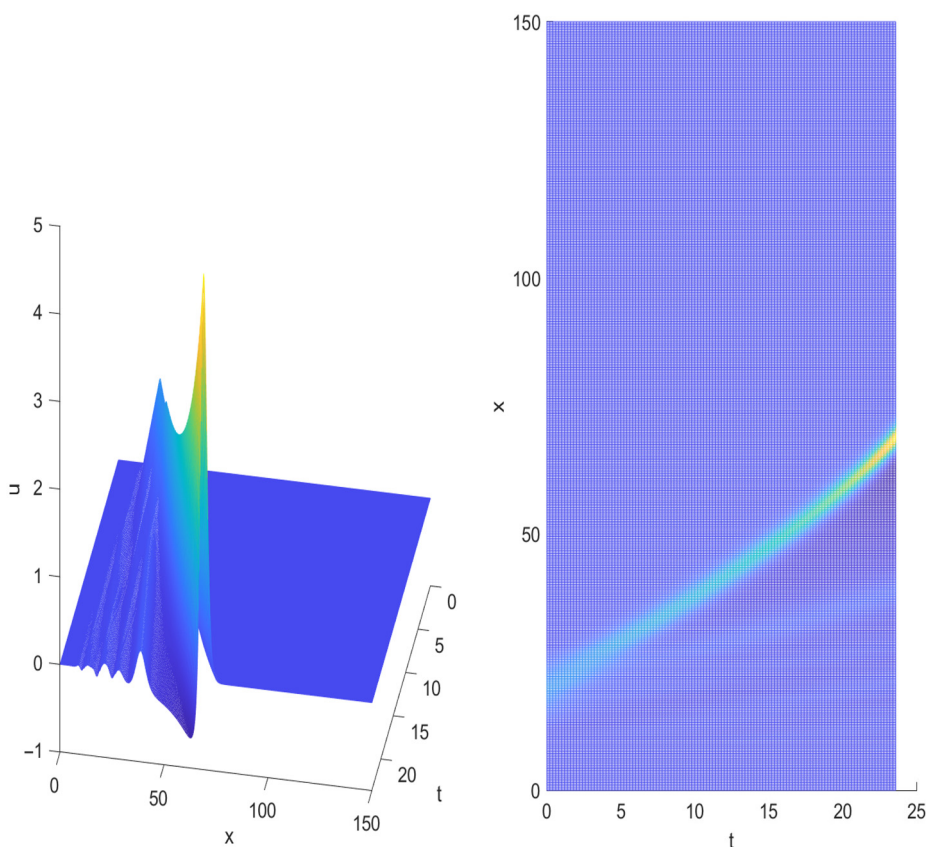

Figure 7.
$u(t, x)$ (left) and
isocontours of $u(t, x)$
(right) for triangular
initial conditions: $A =$
1, $\sigma = 0.05$, $\alpha = 1$,
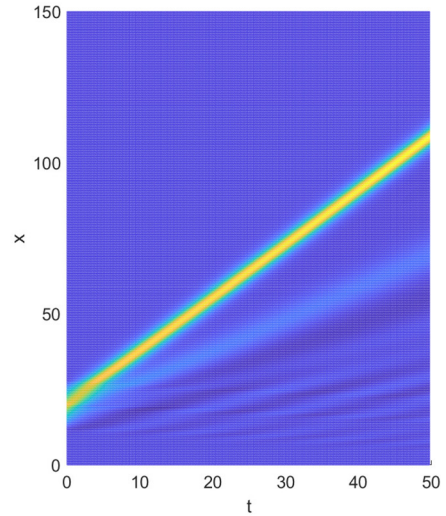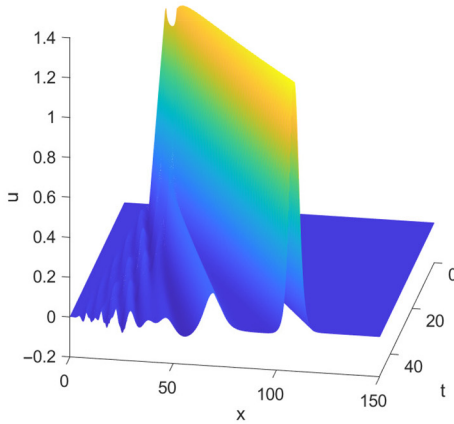$c^2 = 0.1$, $\tau = 0.1$ and
$p = 2$

Source: Figure by authors

ones. This figure also indicates that the maximum amplitude of the leading wave undergoes a longer transition from its initially triangular shape than that for Gaussian conditions. Moreover, whereas the latter results in a relatively smooth transition from the leading wave to the nil value at the upstream boundary, the former is characterized by larger amplitude waves that are generated at different times and whose speed decreases with their distance to the upstream boundary.

Although not shown here, for the same parameters as those of Figure 9, except that $\tau = 0.01$, no blowup has been observed for $t \leq 50$, and the leading wave trajectory exhibits smaller curvature than for Gaussian initial conditions; however, in accord with the results shown in Figures 7 and 8, the number of waves behind the leading one is higher for triangular conditions than for Gaussian ones. Because, as stated previously, both the potential and the stretching energies for the triangular initial conditions are smaller than those for the Gaussian ones, the larger number of oscillations observed between the leading wave front and the upstream boundary for the triangular conditions is caused by their smaller compact support and their nonsmoothness at the vertices of the triangle.

Source: Figure by authors
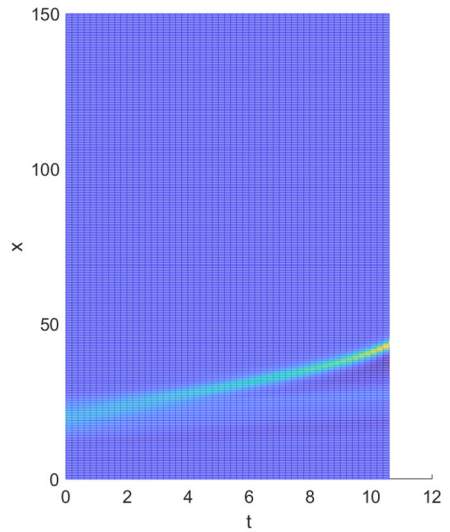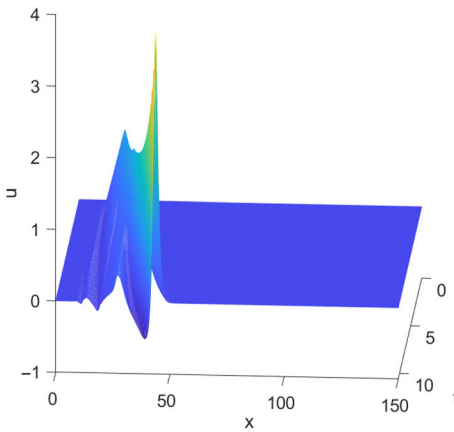
Source: Figure by authors

For $p = 3$, the results presented in Figure 10 indicate that the blowup time is higher than that for Gaussian initial conditions, the first wave behind the leading one has an amplitude larger than that observed in Figure 4 and the number of waves between the leading wave and the upstream boundary is larger than for Gaussian ones. In both Figures 4 and 10, the first wave behind the leading propagating front reaches small negatives values, and the distance between the leading wave and the first one behind it increases as time increases.

Source: Figure by authors

For $\sigma = 0.1$, the results of the numerical experiments reported in Figure 11 for triangular conditions show similar trends to those observed in Figure 5 for Gaussian conditions, but the latter results in smaller blowup times than the former, because of the larger value of $|u_x(0, x)|$ and the number of waves between the leading propagating wave and the upstream boundary is larger for triangular conditions than for Gaussian ones. Moreover, the first and

Source: Figure by authors

second waves behind the leading one have the same shape for those types of boundary conditions.

For $\sigma = 0.05$, the results presented in Figure 12 indicate that, although the blowup time and the number of oscillations behind the leading wave are both larger for triangular conditions than for Gaussian ones (cf. Figure 6), there are marked differences on the waves that appear between the leading one and the upstream boundary; for Gaussian conditions, the waves behind the leading propagating wave are characterized by positive values of $u(t, x)$, whereas those for triangular ones have a higher frequency and reach both positive and negative values. As stated above, this is again a consequence of the fact that triangular conditions have smaller compact support and are not differentiable at the vertices of the triangle.

3.3 Results for rectangular initial conditions

The results reported in this section correspond to rectangular conditions and, unless otherwise stated, the same parameters as those of Figures 1–6 and Figures 7–12 for Gaussian and triangular initial conditions, respectively, so that a comparison between those figures and the ones presented in this section allows to assess the effects of the smoothness of the initial conditions on the wave dynamics and blowup time.

Because comparisons between the results obtained with Gaussian and triangular conditions have already been reported in the previous section, most of the comparisons reported in this section are concerned with the blowup times for Gaussian and rectangular initial conditions.

As indicated in the previous section, for rectangular conditions, $u(0, x)$ exhibits jump discontinuities of absolute value equal to A at $x_0 \pm B$. If the rectangular initial conditions are regularized and replaced by trapezoidal ones which are continuous and piecewise smooth, and the change of $|u(0, x)|$ from 0 to A is assumed to take place in an interval of length equal to grid size, Δx, then the maximum value of the regularized $|u_x(0, x)|$ is equal to $10A$ for the
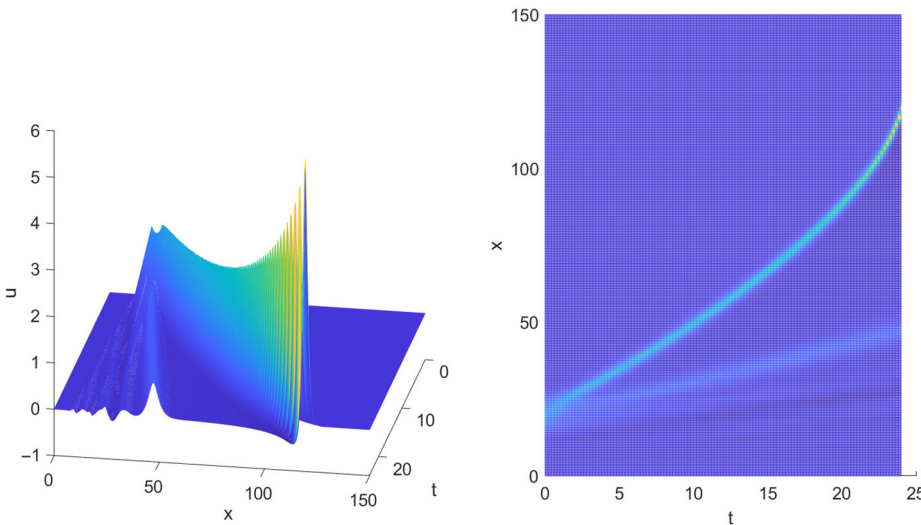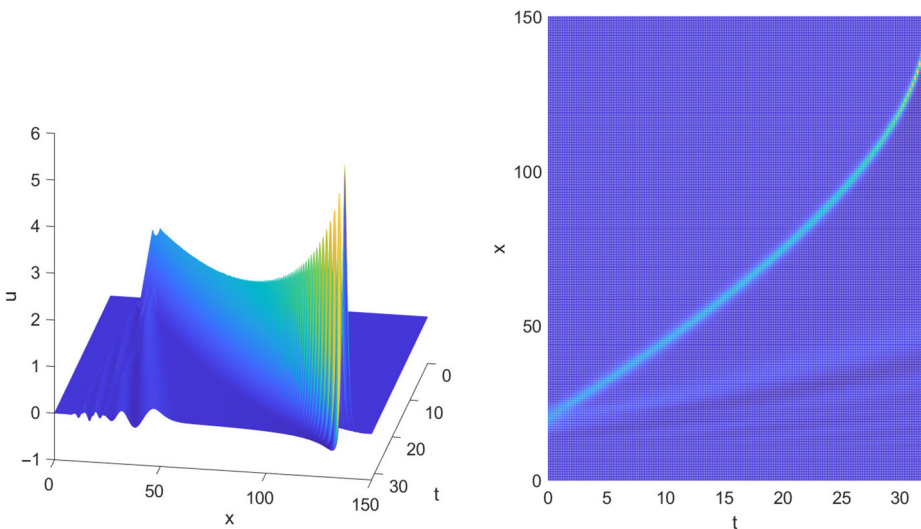

Figure 12.
$u(t, x)$ (left) and isocontours of $u(t, x)$ (right) for triangular initial conditions: $A = 1.5$, $\sigma = 0.05$, $\alpha = 1$, $c^2 = 0.1$, $\tau = 0.01$ and $p = 3$

Source: Figure by authors

grid size used in the calculations reported here. For $A = 1$ and 1.5, these maximum values correspond to slopes equal to 84° and 86°, respectively.

Figure 13 clearly shows that the transition from the rectangular initial conditions to a leading propagating wave front is quite rapid and results in the formation of a complex wave pattern between the leading wave and the upstream boundary; the rectangular initial conditions and their evolution into a complex pattern can be observed clearly in the background of Figure 13. This complex pattern is a consequence of the fact that $u(0, x)$ has no classical derivatives at the vertical sides of the rectangular initial conditions used in this study, as indicated in Section 2.3.

The blowup time for Figure 13 is smaller than that for Figure 1; the latter shows a relatively smooth transition from the back of the leading propagating wave to the upstream boundary, whereas the former exhibits a fast and complex transition characterized by large amplitude waves that move slowly toward but do not reach the downstream boundary.

Figure 14, which corresponds to the same parameter values as those of Figure 13 except that $c^2 = 1$, clearly shows the transition from the rectangular initial conditions to the leading wave, as well as the formation of waves of smaller amplitude between the leading propagating wave and the upstream boundary. Note that, for the same value of c, an increase of τ results in an increase of μ, i.e. for the same value of c, an increase of τ results in increases of both inertia and viscosity. The increase of inertia results in longer blowup times as clearly seen in Figures 13 and 14, while the increase of μ can be observed in both the larger curvature of the leading wave front and the smaller number, smaller frequency and smaller amplitude of the waves that are formed between the leading propagating front and the upstream boundary.

Figures 13 and 14 correspond to $\mu = 0.01$ and 0.1, respectively, and show that, despite the fact that μ is ten times larger in Figure 14 than in Figure 13, the blowup time only increases by about 26% as μ is increased from 0.01 to 0.1, thus indicating that the viscosity coefficient does not play as much as a role on the wave dynamics and blowup time for
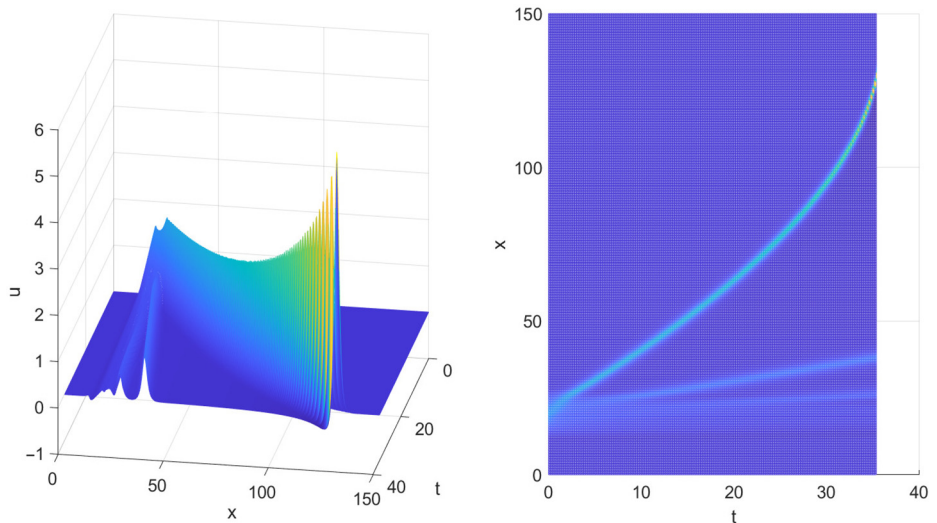

Figure 13.
$u(t, x)$ (left) and isocontours of $u(t, x)$ (right) for rectangular initial conditions: $A = 1$, $\sigma = 0.05$, $\alpha = 1$, $c^2 = 0.1$, $\tau = 0.1$ and $p = 2$

Source: Figure by authors

Figure 14.
$u(t, x)$ (left) and
isocontours of $u(t, x)$
(right) for rectangular
initial conditions: $A = 1$, $\sigma = 0.05$, $\alpha = 1$,
$c^2 = 1$, $\tau = 0.1$ and
$p = 2$

Source: Figure by authors

rectangular initial conditions. However, μ is of paramount importance on determining the wave dynamics between the leading wave and the upstream boundary as discussed in the previous paragraph. In fact, as indicated previously, an increase of μ may result in negative values of β that, in turn, may result in an increase of $E(t)$ [cf. equation (8)].

For $\tau = 0.01$, the results presented in Figure 15 indicate that there is an initial transition region where the rectangular conditions evolve into a leading propagating wave; this

Figure 15.
$u(t, x)$ (left) and
isocontours of $u(t, x)$
(right) for rectangular
initial conditions: $A = 1$, $\sigma = 0.05$, $\alpha = 1$,
$c^2 = 0.1$, $\tau = 0.01$ and
$p = 2$

Source: Figure by authors

transition period is larger than that observed in Figure 2 for Gaussian conditions. After this transition, the leading wave propagates at an almost constant speed for both Gaussian and rectangular conditions, as illustrated in Figures 2 and 15, respectively.

Figure 15 also shows that a complex wave pattern appears between the leading wave and the upstream boundary; this pattern is characterized by two almost stationary waves that emanate from the vertical sides of the initial rectangle and are almost parallel to the upstream boundary. Between the rightmost of these two waves and the leading propagating one, there are traveling waves whose amplitude increases as the distance from the upstream boundary increases. This is in marked contrast with the constant-speed propagating waves observed between the leading wave and the upstream boundary for the Gaussian conditions illustrated in Figure 2.

For $p = 3$, the blowup time corresponding to Figure 16 is about 58% that of Figure 3 in accord with the fact that the rectangular initial conditions are not differentiable at the locations of the vertical sides of the rectangle; as indicated in Section 2, u_x is a Dirac's delta function at these locations for the rectangular conditions. Figure 16 also clearly illustrates both the two almost stationary waves generated at the vertical sides of the initial rectangle and the complex wave pattern between the upstream boundary and leading wave front.

For the same values of the parameters as those of Figure 16 except that $\tau = 0.01$, Figure 17 shows that blowup occurs at a much larger time than in Figure 16, the leading wave front exhibits a curvature that increases with time, and the waves formed between the rightmost stationary wave and the leading one propagate with positive speed toward the downstream boundary, but the two stationary waves that are formed at the locations of the vertical sides of the rectangular initial conditions are not clearly seen. Figure 17 also illustrates the transition from the rectangular initial conditions to the leading wave.

The results presented in Figure 18 indicate that blowup occurs earlier than in Figure 4 and that two almost stationary waves similar to the ones previously discussed are formed at the vertical sides of the rectangular initial conditions. Figure 18 also illustrates the presence
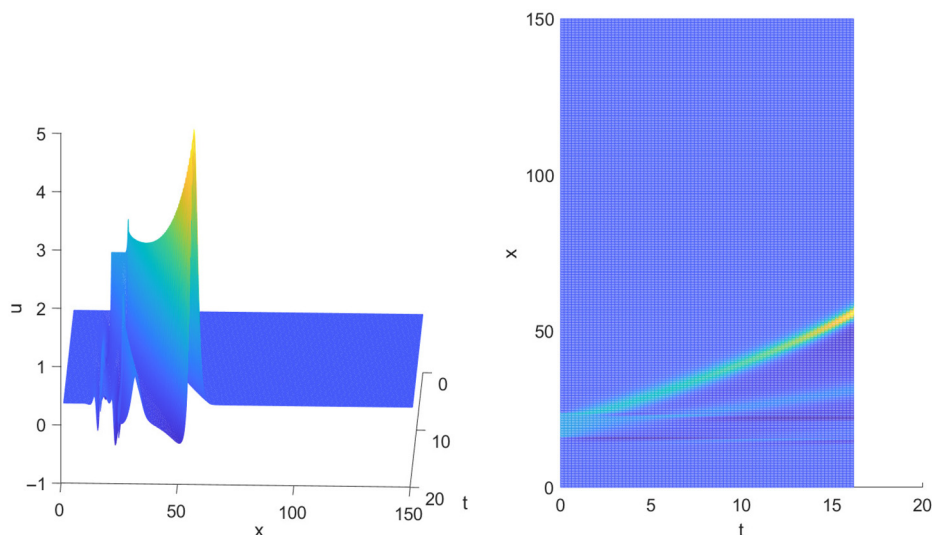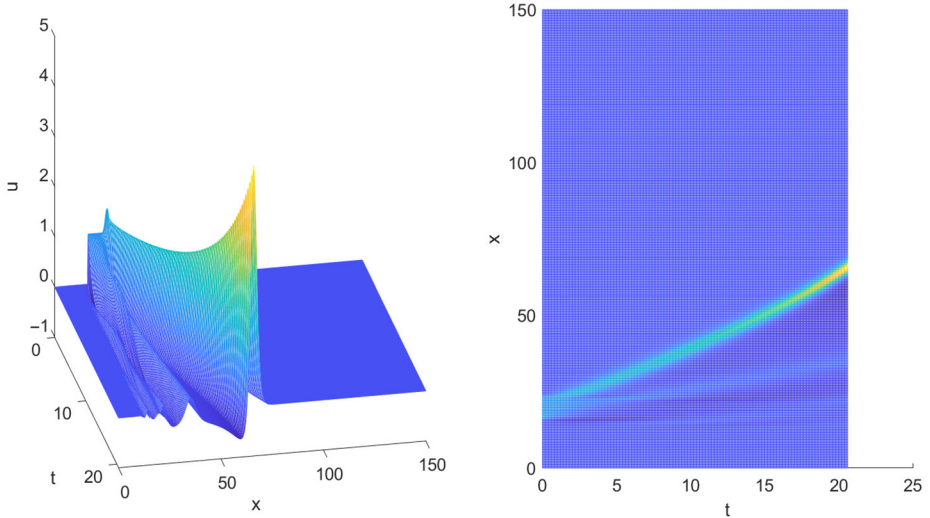

Source: Figure by authors

Figure 16.
$u(t, x)$ (left) and
isocontours of $u(t, x)$
(right) for rectangular
initial conditions: $A =$
$1, \sigma = 0.05, \alpha = 1,$
$c^2 = 0.1, \tau = 0.1$ and
$p = 3$

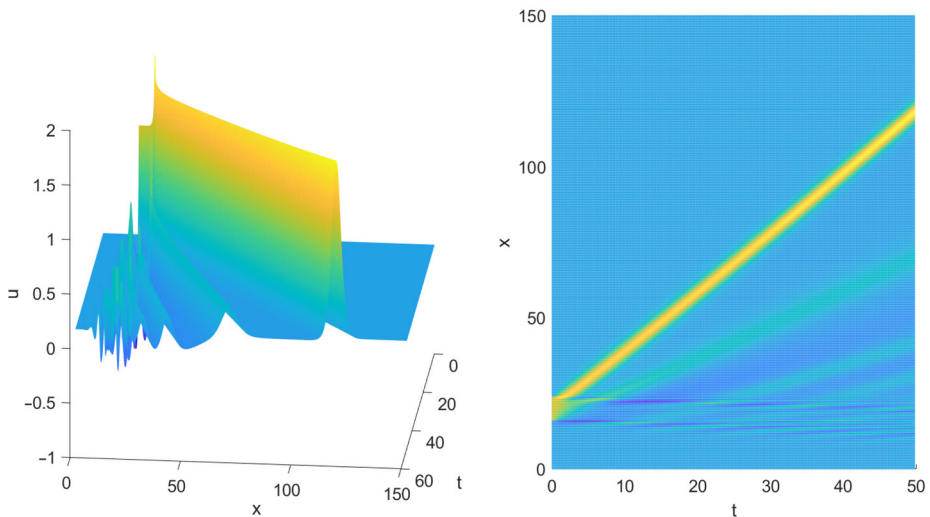**Figure 17.**
$u(t, x)$ (left) and
isocontours of $u(t, x)$
(right) for rectangular
initial conditions: $A =$
$1, \sigma = 0.05, \alpha = 1,$
$c^2 = 0.1, \tau = 0.01$
and $p = 3$

Source: Figure by authors

Figure 18.
$u(t, x)$ (left) and
isocontours of $u(t, x)$
(right) for rectangular
initial conditions: $A =$
$1.5, \sigma = 0.05, \alpha = 1,$
$c^2 = 0.1, \tau = 0.01$
and $p = 3$

Source: Figure by authors

of two right-propagating waves between the stationary waves and the leading one. This figure also shows that there are very large amplitude oscillations between the upstream boundary and the leading wave, and the distance between the leading wave and the first one behind it increases with time.

A comparison between Figures 18 and 4 clearly indicates that the main difference in wave propagation between the results corresponding to rectangular and Gaussian

conditions, respectively, occurs between the leading wave and the upstream boundary and is caused by the nonsmoothness of the rectangular initial conditions.

Figure 19 corresponds to the same values of the parameters as those of Figure 5 and shows a blowup time that is 46% smaller and a larger number of high amplitude waves between the leading wave and the upstream boundary than those for Gaussian conditions. Figure 19 also shows that the back of the leading propagating wave may reach negative values which are in magnitude much smaller than those of the waves located between the upstream boundary and the rightmost almost stationary wave. The curvature of the leading wave front presented in Figure 19 is larger than that of Figure 5.

Similar trends to those shown in Figure 19 are illustrated in Figure 20 that corresponds to $\alpha = 0.1$. The blowup time for Figure 20 is 47.53% that shown in Figure 6; the secondary waves formed between the upstream boundary and the leading propagating wave are mostly characterized by $u(t, x) \geq 0$ for the Gaussian initial conditions, whereas those of Figure 20 exhibit large positive and negative values which are in magnitude larger than those shown in Figure 6. This is again caused by the nonsmoothness of the rectangular initial conditions as one may observe on the background of Figure 20 (left) and in previous figures shown in this section.

3.4 Wave dynamics and blowup

In the three previous sections, some results on the wave dynamics of equation (1) subject to the three initial conditions considered in this paper were presented as functions of space and time until either blowup or the collision of the leading wave with the downstream boundary for rectangular initial conditions occurred. In those sections, the projection of $u(t, x)$ on the (t, x) plane was also shown to illustrate the wave propagation and the wave curvature.

As indicated previously, because the initial conditions considered in Sections 3.1–3.3 do not correspond to those for which a solitary wave solution of equation (1) exists, the results shown in those sections clearly illustrate the presence of a leading wave propagating toward
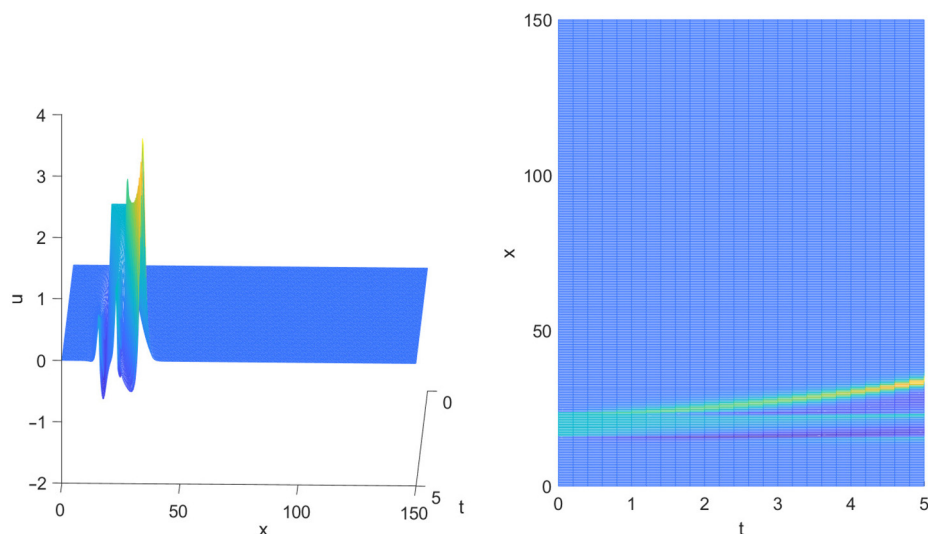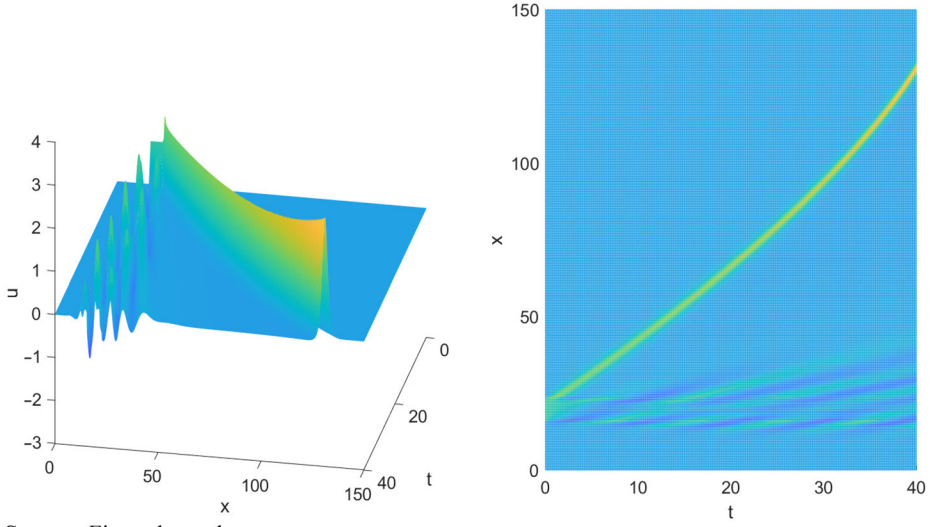

Source: Figure by authors

Figure 19.
$u(t, x)$ (left) and isocontours of $u(t, x)$ (right) for rectangular initial conditions: $A = 1.5$, $\sigma = 0.1$, $\alpha = 1$, $c^2 = 0.1$, $\tau = 0.01$ and $p = 3$
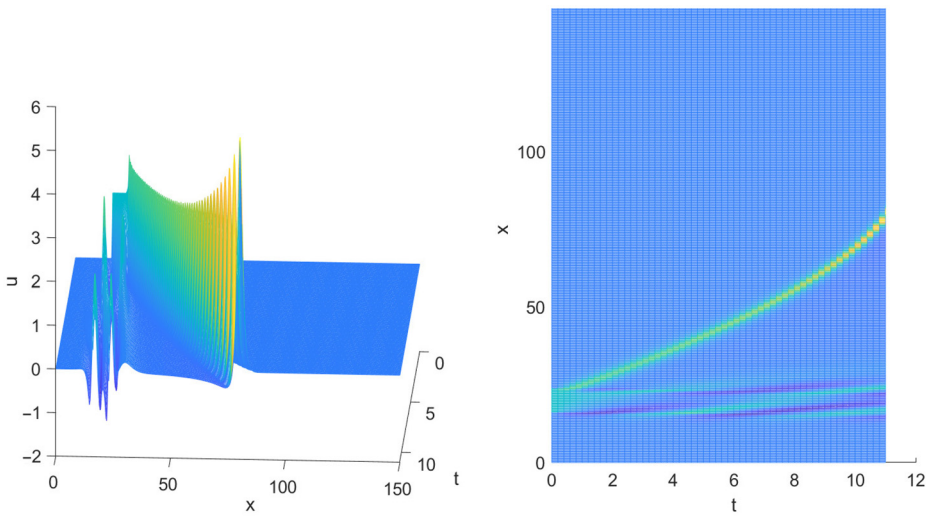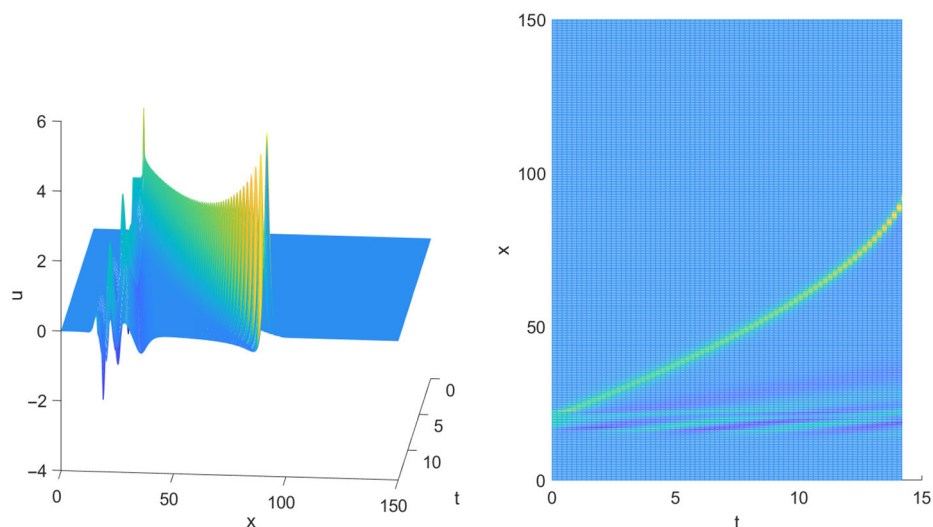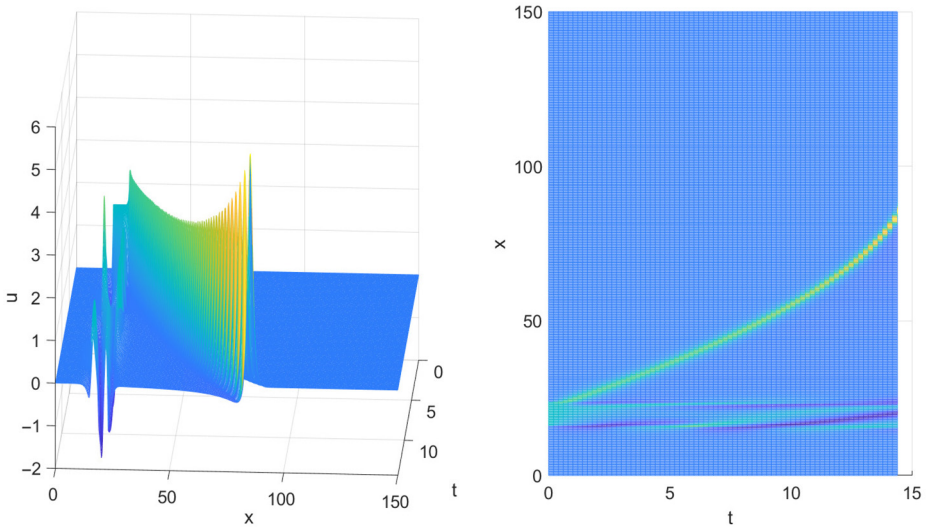
Figure 20.
$u(t, x)$ (left) and
isocontours of $u(t, x)$
(right) for rectangular
initial conditions: $A =$
1.5, $\sigma = 0.05$, $\alpha = 0.1$,
$c^2 = 0.1$, $\tau = 0.01$ and
$p = 3$

Source: Figure by authors

the downstream boundary and complex wave phenomena between this leading wave and the upstream boundary.

In this section, some snapshots of the results presented in Sections 3.1–3.3 are presented for the three initial conditions studied in this paper to both illustrate and emphasize the effects of these conditions on the wave dynamics until either blowup or wave collision with the downstream boundary occurs. Because, as shown in Sections 3.1–3.3, the smallest blowup time corresponds to that of the rectangular initial conditions, only the results corresponding to times smaller than or equal to that blowup time are presented in the following figures for the three initial conditions studied in this paper.

Figure 21 has been obtained from Figures 1, 7 and 13 and indicates that no blowup occurs for $t \leq 50$. For initial Gaussian conditions, Figure 21 (top left) indicates that the wave's height increases as time increases, and a train of small amplitude waves is formed behind the leading propagating wave; the amplitude of this wave train increases as the leading wave front approaches the downstream boundary.

Similar trends to the ones described for Gaussian conditions can be observed for the triangular initial conditions illustrated in Figure 21 (top right), but in this case, the wave train formed behind the leading wave front is closer to the upstream boundary.

The results for rectangular initial conditions presented in Figure 21 (bottom left) show similar trends to those for Gaussian and triangular conditions; however, a complex high-frequency wave pattern is formed near the locations where the initial conditions are specified and $u(t, x)$ is not differentiable. The results presented in Figure 21 (bottom left) also show that waves propagate from $x_0 - B$ toward the upstream boundary, but the amplitude of these waves decreases as the distance to this boundary decreases, and the frequency of these waves is higher than that of the waves observed for $x > x_0 + B$.

At $t = 50$, the results presented in Figure 21 (bottom right) show that the leading wave amplitude and speed are largest for the rectangular initial conditions and smallest for the triangular ones; they also show that complex wave patterns are located around the locations
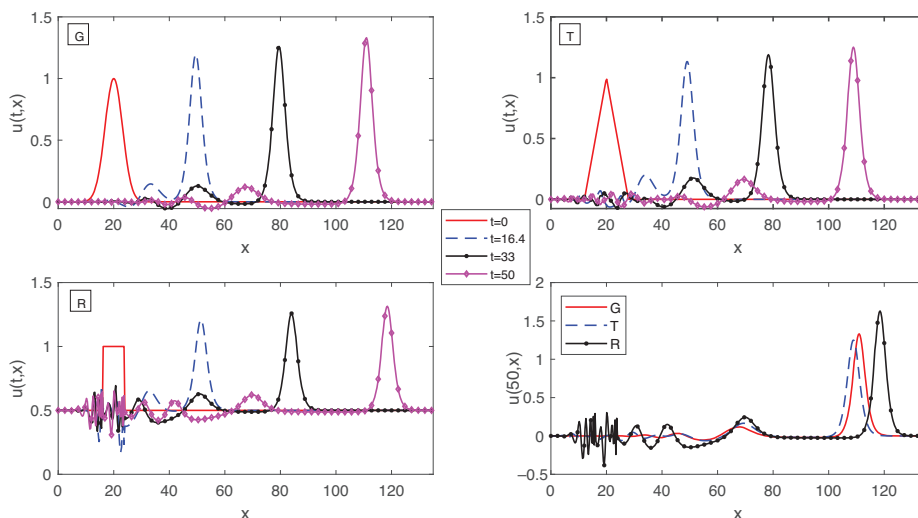
Source: Figure by authors

where the rectangular and triangular initial conditions were specified, and the complexity of the wave train is larger for rectangular than for triangular conditions, i.e. the complexity of the wave pattern behind the leading propagating front increases as the nonsmoothness of the initial conditions is increased.

Figure 22 shows results obtained from Figures 2, 8 and 15 and exhibits similar trends to those observed in Figure 21. Note that, for the values of the parameters used to obtain Figure 22, the rectangular conditions resulted in blowup at $t \approx 16.4$.

Figure 22 (bottom left) shows that the amplitude of the leading wave increases as time increases, both the complexity and the amplitude of the wave pattern behind the leading wave increase as the nonsmoothness of the initial conditions is increased, both the amplitude and the speed of the leading wave at $t = 16.4$ are largest for the rectangular conditions and smallest for the triangular ones and the smoothness of the wave train that appears behind the leading wave front increases as the smoothness of the initial conditions is increased.

Some snapshots of the results presented in Figures 3, 9 and 17 are illustrated in Figure 23. It must be noted that, for the values of the parameters used to obtain Figure 23, wave collision with the downstream boundary was observed for the rectangular initial conditions, and only times smaller than the collision time have been considered to not account for the effect of the boundary conditions on the wave propagation and blowup time.

The results illustrated in Figure 23 exhibit similar trends to those of Figure 21, except that the amplitude and speed of the leading front is smaller for the latter; the amplitude of the complex wave pattern observed near where the initial conditions are specified is larger in Figure 23 than in Figure 21, whereas the wave frequency exhibits the opposite trend. This is due to the relaxation time which is equal to $\tau = 0.01$ in Figure 23 and 0.1 in Figure 21 and, therefore, $\mu = 0.01$ and 0.1 in Figures 23 and 21, respectively, i.e. viscous effects are larger in Figure 23 than in Figure 21; it is also due to the higher advection nonlinearity, i.e. $p = 3$ and 2 in Figures 23 and 21, respectively.

Figure 22.
$u(t, x)$ for Gaussian
(G), triangular (T) and
rectangular (R) initial
conditions: $A = 1$,
$\sigma = 0.05$, $\alpha = 1$,
$c^2 = 0.1$, $\tau = 0.01$ and
$p = 2$

Source: Figure by authors

Figure 23.
$u(t, x)$ for Gaussian
(G), triangular (T) and
rectangular (R) initial
conditions: $A = 1$,
$\sigma = 0.05$, $\alpha = 1$,
$c^2 = 0.1$, $\tau = 0.01$ and
$p = 3$

Source: Figure by authors

The results illustrated in Figure 24 correspond to snapshots taken from Figures 4, 10 and 18 and exhibit blowup at early times. For Gaussian initial conditions, Figure 24 (top left) shows the steepening of the leading front as time increases, as well as the presence of a relative minimum at $t \approx 1.8$ when blowup is observed for the rectangular initial conditions. A similar steepening and the formation of a relative minimum are also observed for
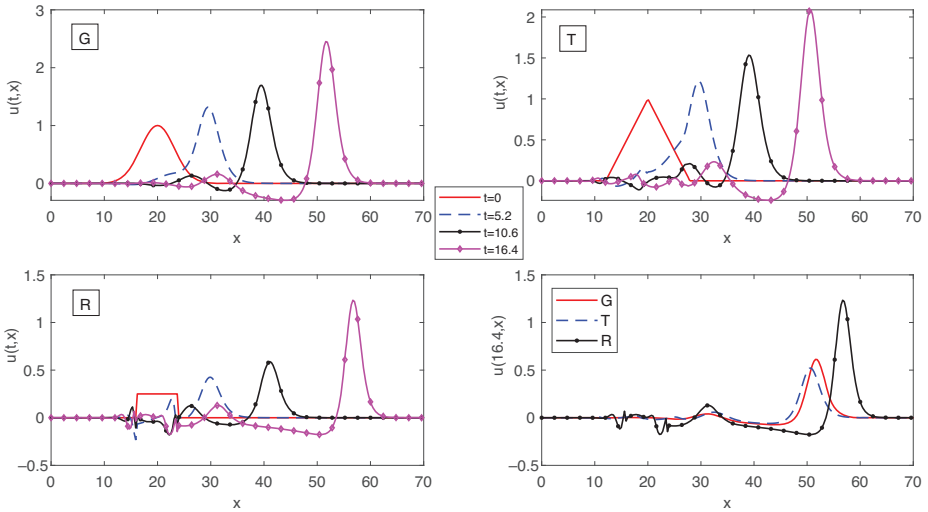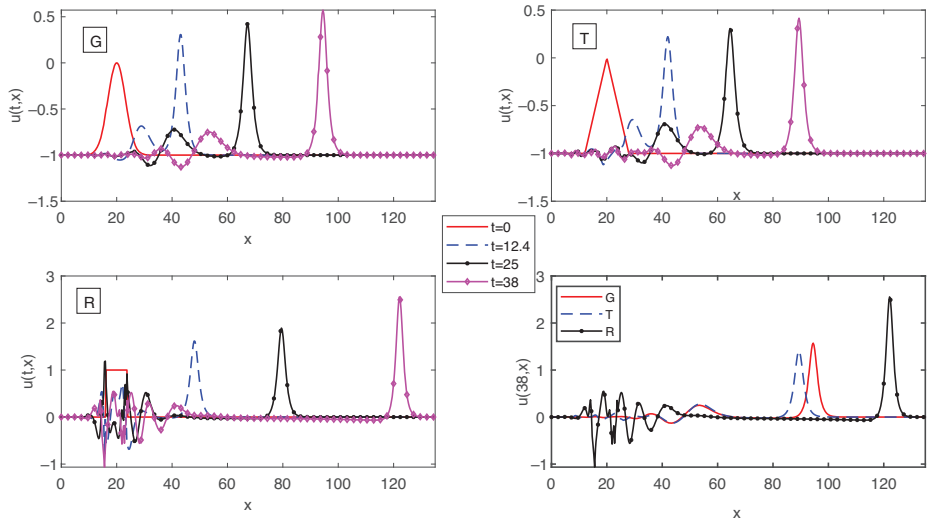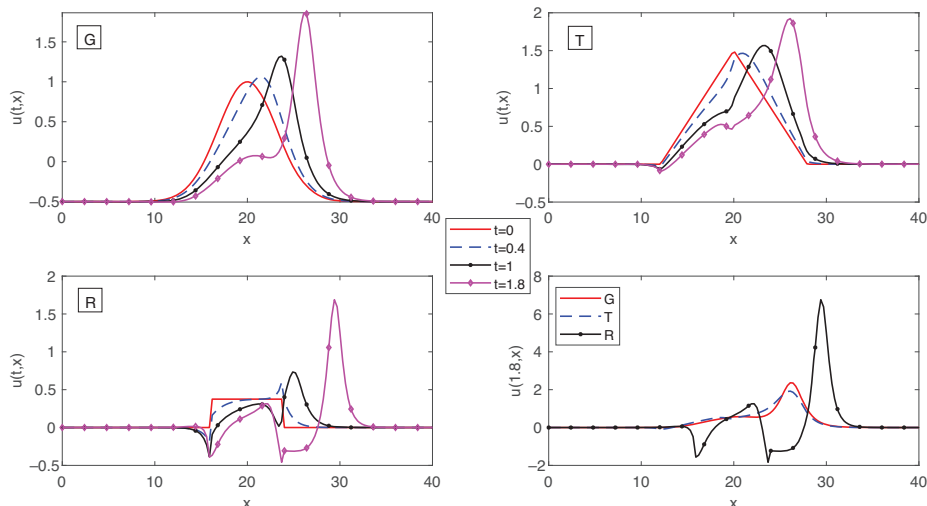
Figure 24.
$u(t, x)$ for Gaussian
(G), triangular (T) and
rectangular (R) initial
conditions: $A = 1.5$,
$\sigma = 0.05$, $\alpha = 1$,
$c^2 = 0.1$, $\tau = 0.01$ and
$p = 3$

Source: Figure by authors

triangular initial conditions, which also result in negative values of $u(t, x)$ at the location of the left vertex of the triangle used in the initial condition as indicated in Figure 24 (top right). By way of contrast, for rectangular initial conditions, steepening is observed in the lee side of leading wave front as well as in the wave that is formed at the left vertical edge of the rectangle used for the initial conditions.

A comparison among the results presented in Figures 21–24 clearly indicates that, if the blowup time is small, the train of waves behind the leading front does not consist of many waves for Gaussian and triangular initial conditions, whereas it consists of two almost stationary waves located at the vertical edges of the rectangle for rectangular initial conditions and the amplitude of these waves increases with time. This is not surprising if the blowup time is smaller than the diffusion and dispersion times because, in this case, there is not enough time for the formation, diffusion and dispersion of waves.

Similar results to those presented in Figure 24 have also been found for Figures 5, 11 and 19 and Figures 6 and 20 as well for the results that exhibit blowup in finite time summarized in Tables 1–4, but are not reported here.

3.5 Blowup times
A summary of the blowup times obtained with the finite difference method described in the previous section is presented in Tables 1–4; this summary is a very brief description of a much larger set of numerical experiments that have been performed to analyze the effect of the parameters of equation (1) and the amplitude and width of the three types of initial conditions considered in this study, on blowup.

In Tables 1–4, the results of numerical experiments that do not result in blowup for $t \leq$ 50 are also included so that the reader may observe the effects that the parameters of equation (1) and the initial boundary conditions have on the development of time singularities. For example, for the initial Gaussian conditions with $c^2 = 0.1$ and $p = 2$ shown in Table 1, neither blowup nor wave collision with the boundaries occurs for $\tau = 0.001$ and

Gaussian	p = 2			p = 3		
	$\tau = 0.001$	$\tau = 0.01$	$\tau = 0.1$	$\tau = 0.001$	$\tau = 0.01$	$\tau = 0.1$
$c^2 = 0.1$	nbu-nwc	nbu-nwc	21.7118	nbu-nwc	nbu-nwc	9.0368
$c^2 = 1$	nbu-nwc	nbu-nwc	27.7538	nbu-nwc	nbu-nwc	10.8311
$c^2 = 10$	nbu-nwc	nbu-nwc	nbu-nwc	nbu-nwc	nbu-nwc	nbu-nwc
Triangular	$\tau = 0.001$	$\tau = 0.01$	$\tau = 0.1$	$\tau = 0.001$	$\tau = 0.01$	$\tau = 0.1$
$c^2 = 0.1$	nbu-nwc	nbu-nwc	23.9071	nbu-nwc	nbu-nwc	10.8283
$c^2 = 1$	nbu-nwc	nbu-nwc	30.8546	nbu-nwc	nbu-nwc	13.2703
$c^2 = 10$	nbu-nwc	nbu-nwc	nbu-nwc	nbu-nwc	nbu-nwc	nbu-nwc
Rectangular	$\tau = 0.001$	$\tau = 0.01$	$\tau = 0.1$	$\tau = 0.001$	$\tau = 0.01$	$\tau = 0.1$
$c^2 = 0.1$	nbu-nwc	nbu-nwc	16.4509	nbu-nwc	nbu-wc	5.2732
$c^2 = 1$	nbu-nwc	nbu-nwc	20.8007	nbu-nwc	nbu-wc	6.1748
$c^2 = 10$	nbu-nwc	nbu-nwc	nbu-nwc	nbu-nwc	nbu-nwc	nbu-nwc

Table 1.
Blowup times for $\alpha = 1$, $a = 1$ and $\sigma = 0.05$

Notes: nbu and nwc denote that no blowup and no wave collision with the boundaries occur for $t \leq 50$, respectively; wc indicates that wave collision with the boundaries occurs for $t \leq 50$
Source: Table by authors

Gaussian	p = 2			p = 3		
	$\tau = 0.001$	$\tau = 0.01$	$\tau = 0.1$	$\tau = 0.001$	$\tau = 0.01$	$\tau = 0.1$
$c^2 = 0.1$	nbu-nwc	nbu-nwc	11.8965	nbu-wc	19.9554	3.0721
$c^2 = 1$	nbu-nwc	nbu-nwc	13.6590	nbu-wc	21.2452	3.2303
$c^2 = 10$	nbu-nwc	nbu-nwc	nbu-nwc	nbu-wc	nbu-nwc	nbu-nwc
Triangular	$\tau = 0.001$	$\tau = 0.01$	$\tau = 0.1$	$\tau = 0.001$	$\tau = 0.01$	$\tau = 0.1$
$c^2 = 0.1$	nbu-nwc	nbu-nwc	13.2314	nbu-nwc	24.2558	3.7349
$c^2 = 1$	nbu-nwc	nbu-nwc	15.2873	nbu-wc	26.1121	3.9541
$c^2 = 10$	nbu-nwc	nbu-nwc	nbu-nwc	nbu-wc	nbu-nwc	nbu-nwc
Rectangular	$\tau = 0.001$	$\tau = 0.01$	$\tau = 0.1$	$\tau = 0.001$	$\tau = 0.01$	$\tau = 0.1$
$c^2 = 0.1$	nbu-nwc	nbu-wc	8.9945	nbu-wc	11.3606	1.8277
$c^2 = 1$	nbu-nwc	nbu-wc	10.2957	nbu-wc	11.8246	1.9267
$c^2 = 10$	nbu-nwc	nbu-nwc	nbu-nwc	nbu-wc	23.8871	4.5861

Table 2.
Blowup times for $\alpha = 1$, $a = 1.5$ and $\sigma = 0.05$

Notes: nbu and nwc denote that no blowup and no wave collision with the boundaries occur for $t \leq 50$, respectively; wc indicates that wave collision with the boundaries occurs for $t \leq 50$
Source: Table by authors

0.01, and $t \leq 50$, but blowup occurs for $\tau = 0.1$. On the other hand, for the same initial conditions with $c^2 = 0.1$ and $p = 3$, blowup does not occur but wave collision with the downstream boundary takes place at $t \leq 50$ for $\tau = 0.001$, whereas blowup occurs at $t < 50$ for $\tau = 0.01$ and 0.1. Moreover, the last column of Table 1, for example, shows the dependence of the blowup time on $\mu = \pi c^2$, for $\alpha = 1$, $p = 3$, $A = 1$, $\sigma = 0.05$ and $\tau = 0.1$ for the Gaussian, triangular and rectangular initial conditions studied numerically in this paper, and indicates that the blowup time increases as c^2 or μ is increased.

Tables 1–3 correspond to $\alpha = 1$. Table 1 shows that no blowup occurs for $A = 1$, $\sigma = 0.05$, $c^2 = 0.1$, 1 and 10, $\tau = 0.001$ and 0.01 and $p = 2$ and 3, for $t \leq 50$ and the three initial conditions studied in this paper. Note that, for a fixed value of τ, an increase of c^2 corresponds to an increase of the viscosity coefficient, μ, and the viscous dissipation.

Gaussian	$\tau = 0.001$	$p = 2$ $\tau = 0.01$	$\tau = 0.1$	$\tau = 0.001$	$p = 3$ $\tau = 0.01$	$\tau = 0.1$
$c^2 = 0.1$	nbu-nwc	nbu-nwc	13.6483	nbu-wc	26.7420	3.4850
$c^2 = 1$	nbu-nwc	nbu-nwc	16.3587	nbu-wc	29.1663	3.7723
$c^2 = 10$	nbu-nwc	nbu-nwc	nbu-nwc	nbu-nwc	nbu-nwc	nbu-nwc
Triangular	$\tau = 0.001$	$\tau = 0.01$	$\tau = 0.1$	$\tau = 0.001$	$\tau = 0.01$	$\tau = 0.1$
$c^2 = 0.1$	nbu-nwc	nbu-nwc	14.8974	nbu-nwc	32.0642	4.1601
$c^2 = 1$	nbu-nwc	nbu-nwc	17.9788	nbu-nwc	41.9600^2	4.5521
$c^2 = 10$	nbu-nwc	nbu-nwc	nbu-nwc	nbu-nwc	nbu-nwc	nbu-nwc
Rectangular	$\tau = 0.001$	$\tau = 0.01$	$\tau = 0.1$	$\tau = 0.001$	$\tau = 0.01$	$\tau = 0.1$
$c^2 = 0.1$	nbu-nwc	nbu-nwc	10.2667	nbu-wc	14.4290	1.9415
$c^2 = 1$	nbu-nwc	nbu-nwc	12.1459	nbu-wc	15.1845	2.0683
$c^2 = 10$	nbu-nwc	nbu-nwc	nbu-nwc	nbu-wc	nbu-wc	nbu-nwc

Notes: nbu and nwc denote that no blowup and no wave collision with the boundaries occur for $t \leq 50$, respectively; wc indicates that wave collision with the boundaries occurs for $t \leq 50$
Source: Table by authors

1217

Table 3. Blowup times for $\alpha = 1$, $a = 1.5$ and $\sigma = 0.1$

Gaussian	$\tau = 0.001$	$p = 2$ $\tau = 0.01$	$\tau = 0.1$	$\tau = 0.001$	$p = 3$ $\tau = 0.01$	$\tau = 0.1$
$\alpha = 0.1$	nbu-nwc	nbu-nwc	18.3020	nbu-nwc	28.1889	3.9269
$\alpha = 1$	nbu-nwc	nbu-nwc	11.8965	nbu-wc	19.9554	3.0721
$\alpha = 2$	nbu-wc	nbu-wc	8.5080	nbu-wc	15.4992	2.5315
Triangular	$\tau = 0.001$	$\tau = 0.01$	$\tau = 0.1$	$\tau = 0.001$	$\tau = 0.01$	$\tau = 0.1$
$\alpha = 0.1$	nbu-nwc	nbu-nwc	20.8075	nbu-nwc	35.7121	4.9117
$\alpha = 1$	nbu-nwc	nbu-nwc	13.2314	nbu-wc	24.2558	3.7349
$\alpha = 2$	nbu-wc	nbu-wc	9.3524	nbu-wc	18.4447	3.0334
Rectangular	$\tau = 0.001$	$\tau = 0.01$	$\tau = 0.1$	$\tau = 0.001$	$\tau = 0.01$	$\tau = 0.1$
$\alpha = 0.1$	nbu-nwc	nbu-nwc	13.4716	nbu-wc	14.7502	2.2051
$\alpha = 1$	nbu-nwc	nbu-wc	8.9945	nbu-wc	11.3606	1.8277
$\alpha = 2$	nbu-wc	nbu-wc	6.4833	nbu-wc	9.1956	1.5563

Notes: nbu and nwc denote that no blowup and no wave collision with the boundaries occur for $t \leq 50$, respectively; wc indicates that wave collision with the boundaries occurs for $t \leq 50$
Source: Table by authors

Table 4. Blowup times for $a = 1.5$, $\sigma = 0.05$ and $c^2 = 0.1$

Table 1 also shows that the blowup time increases as c^2 is increased on account of the increase in μ, and decreases as p is increased, i.e. as the degree of the nonlinearity of equation (1) is increased. Note that, for $\mu = \delta = \tau = 0$, equation (1) becomes a first-order, quasilinear, partial differential equation that has an analytical solution and results in the formation of a shock wave in finite time, if $u_x(0, x)$ is negative (Whitham, 1974). Note also that, as stated in Section 2, large values of μ may result in negative values of β, positive values of the fourth term in the right-hand side of equation (5) and increasing values of the potential energy which may lead to blowup in finite time.

The results presented in Table 1 also indicate that the triangular initial conditions result in slightly larger blowup times than the Gaussian ones and that the smallest blowup times

correspond to rectangular initial conditions. Because, as stated in the previous section, the initial mass is the same for the three initial conditions considered in this study, it may be stated that the lack of smoothness of the rectangular initial conditions is a main contributor to the shorter blowup times associated with these conditions. The decrease in blowup time as the nonsmoothness of the initial conditions is increased described above is in accord with Elgindi's mathematical studies of the three-dimensional, inviscid Euler's equations (Elgindi, 2021); this author showed that nonsmooth initial conditions result in blowup and that the question of blowup for smooth initial conditions remains an open problem.

Table 1 also indicates that, for $\tau = 0.1$ and $p = 3$, the blowup times corresponding to the triangular initial conditions are about twice those of the rectangular ones; however, for $\tau = 0.1$ and $p = 2$, the blowup times for the rectangular conditions are about two-thirds of those corresponding to the triangular ones. The blowup times for $p = 2$, $\tau = 0.1$ and Gaussian, triangular and rectangular conditions shown in Table 1 are about twice, twice and thrice, respectively, those for $p = 3$ and $\tau = 0.1$, for $c^2 = 0.1$ and 1. Note that no blowup has been observed for $t \leq 50$, $c^2 = 10$ and $p = 2$ and 3.

In Table 2, some blowup times are presented for the same values of the parameters as those of Table 1, except that $A = 1.5$. This table shows that no blowup occurs for $A = 1.5$, $\sigma = 0.05$, $c^2 = 0.1$, 1 and 10, $\tau = 0.001$ and 0.01 and $p = 2$, and $\tau = 0.001$ and $p = 3$, for $t \leq 50$.

The results shown in Table 2 exhibit the same qualitative trends as those presented in Table 1, except that the blowup times for $p = 2$ and $p = 3$ shown in Table 1 are about twice and thrice greater than those of Table 2, respectively, for $\tau = 0.1$.

For $\tau = 0.1$ and $p = 3$, the blowup times shown in Table 2 do not change substantially as c^2 is increased from 0.1 to 1 for each of the initial conditions considered in this study, and the shortest and largest blowup times correspond to rectangular and triangular, respectively, initial conditions. Table 2 also indicates that no blowup is observed at $t = 50$ for $p = 2$ and 3 and $c^2 = 10$ for the triangular and Gaussian conditions; however, blowup has been observed for the rectangular conditions with $p = 3$, $\tau = 0.1$ and $c^2 = 10$, thus indicating that the increase in viscosity associated with an increase in τ is not able to overcome both the steepness associated with the initial conditions and the nonlinear advection term for $p = 3$ and $\tau = 0.1$.

For $p = 3$, the blowup times observed in Table 2 for $\tau = 0.01$ are about six times larger than those for $\tau = 0.1$, for the Gaussian, triangular and rectangular conditions and $c^2 = 0.1$ and 1. On the other hand, the blowup time for $p = 3$, $c^2 = 10$ and $\tau = 0.01$ is about five times larger than that for $\tau = 0.1$ for the rectangular initial conditions. In addition, the blowup times for $c^2 = 0.1$ and 1, $\tau = 0.1$ and $p = 2$ are about four, four and five times larger than those for $p = 3$ for the Gaussian, triangular and rectangular, respectively, initial conditions.

Similar trends to those illustrated in Tables 1 and 2 are observed in Table 3, which corresponds to $\sigma = 0.1$. Notice that, as indicated in Section 2.3, $\frac{2}{\sqrt{\sigma}}$ is an indication of the width of the Gaussian initial conditions, and, therefore, the width of the initial conditions increases as σ is decreased.

Table 3 shows that the blowup time increases as c^2 is increased for $\tau = 0.1$ and $p = 2$, and for $\tau = 0.01$ and 0.1 and $p = 3$, while it decreases, for $c^2 = 0.1$ and 1, as τ is increased for the three types of initial conditions considered in this study.

For $\tau = 0.1$ and $c^2 = 0.1$ and 1, the blowup times for $p = 2$ shown in Table 3 are about four, four and six times larger than those for $p = 3$ for the Gaussian, triangular and rectangular initial conditions, respectively. However, the blowup times shown in Tables 2 and 3 do not exhibit a clear dependence on σ; in fact, for $\sigma = 0.1$, $p = 3$ and $\tau = 0.001$ and 0.01, the results shown in Table 3 do not show blowup at $t \leq 50$ for $c^2 = 10$, whereas those

presented in Table 2 for the same values of the parameters except that $\sigma = 0.05$ do show blowup in finite time, for $c^2 = 10$.

The increase in blowup time as σ is increased illustrated in Tables 2 and 3 is a main consequence of the broadening of the initial conditions as σ is decreased, i.e. a decrease of $|u_x(0, t)|$ as σ is decreased, and the associated decrease in the stretching energy, $D(t)$ [cf. equation (6)].

The blowup times for $A = 1.5$, $c^2 = 0.1$, $\sigma = 0.05$ and several values of α, τ and p are illustrated in Table 4. This table indicates that, for $\tau = 0.001$ and 0.01 and $p = 2$, and $\tau = 0.001$ and $p = 3$, no blowup occurs for $t \leq 50$ and $\alpha = 0.1$, 1 and 2.

For a fixed value of τ, Table 4 shows that the blowup time decreases as α is increased; for example, for $p = 2$ and $\tau = 0.1$, the blowup time corresponding to $\alpha = 0.1$ is about twice that for $\alpha = 2$, whereas, for $p = 3$, the blowup time for $\alpha = 0.1$ is about one and a half times that for $\alpha = 2$. It must be pointed out that the velocity of the leading wave increases as α is increased and, therefore, the time required by the leading wave to collide with the downstream boundary decreases as α is increased.

Table 4 also indicates that, for $p = 3$, the blowup times corresponding to $\tau = 0.01$ are about seven times larger than those for $\tau = 0.1$, $\alpha = 0.1$, 1 and 2 and the three initial conditions analyzed in this manuscript. Table 4 also shows that the shortest and longest blowup times correspond to rectangular and triangular initial conditions, respectively. Because, for a fixed value of c^2, an increase of τ corresponds to an increase of μ, i.e. an increase of viscous dissipation, the blowup times presented in Table 4 clearly illustrate the competition among inertia, i.e. τu_{tt}, nonlinear steepness associated with nonlinear advection (ϵ and p) and the dissipative effect associated with viscosity (μ). This behavior can also be observed in Table 4 by comparing the blowup times for $p = 2$ with those for $p = 3$ for $\tau = 0.1$, which indicate that the blowup times substantially decrease as p is increased.

It is worth mentioning that an increase of α corresponds to an increase of the (linear) drift toward to the downstream boundary as indicated in equation (1). As a consequence, large values of α may result in the collision of the leading wave front with the downstream boundary at $t < 50$. As stated above, when the leading wave collides with the downstream boundary for $t < 50$, the numerical results were filtered out and only processed for times less than the collision time to ensure that the downstream and upstream boundary conditions do not affect the wave propagation and blowup time.

3.6 Solution growth
In the previous section, the blowup times illustrated in Tables 1–4 have been discussed for $t_{bu} < 50$, i.e. when blowup occurs before $t = 50$. However, these tables also contain information on numerical experiments that do not exhibit blowup for $x \in [0, L]$ and $t \leq 50$; this information is discussed in the present section.

In Tables 1–4, nbu-nwc indicates that neither blowup nor wave collision with the boundaries occurs for $0 \leq t \leq 50$, whereas nbu-wc is used to emphasize that, even though no blowup occurs, waves have collided with either boundary for $t \leq 50$. Note that, for nbu-nwc, blowup may occur for $t > 50$. On the other hand, for nbu-wc, collisions with the right boundary may not occur for $L > 150$ and blowup may take place for $t > 50$.

Because, for both nbu-nwc and nbu-wc, no blowup has been observed using the blowup time criterion and the time interval and spatial domain discussed above, but the solution may blow up at later times, the temporal growth of the solutions may be determined or estimated to assess the likelihood of (or lack thereof) blowup in these cases. To that end, one may determine numerically the value of $\max |u_t(t_2, x)|$, where $\max[\phi] \equiv \max_{0 \leq x \leq L}[\phi]$ and $t_2 \leq 50$ is the largest time for which the downstream boundary conditions do not affect the

wave propagation; however, this value only provides information about the largest value of the time derivative at $t = t_2$. An alternative estimate of the solution temporal growth when there is no blowup for $t \leq 50$ may be obtained by means of $s \equiv [u_{\max}(t_2, x) - u_{\max}(t_1, x)]/(t_2 - t_1)$, where $t_2 - t_1 \geq 20$ and $t_2 \leq 50$. Note that, if the leading wave does not collide with the downstream boundary and there is no blowup for $0 \leq t \leq 50$, then $t_2 = 50$. Note also that, if $t_{bu} < 50$, $u(t, x)$ shows a rapid increase in time as $t \to t_{bu}^-$ and, therefore, the value of s may be used as a second indicator of blowup. Recall that the blowup time criterion used in Sections 3.1–3.4 corresponds to $|u(t_{bu}, x)| \geq 5A|$.

Note that negative values of s indicate that $u_{\max}(t, x)$ decreases as t increases in accord with some of the results presented in Part I for equation (1) subject to smooth initial conditions which are of either Gaussian type or correspond to the exact solution of the inviscid, generalized RLW equation, when no blowup occurs (Ramos and García López, 2020).

From the numerical experiments performed to determine the blowup times reported in Table 1, $p = 2$ and $c^2 = 1$, the values of $u_{\max}(t^*, x)$ ($t^* \in [t_1, t_2]$) and s ($s > 0$) for $\tau = 0.001$ and 0.1 have been found to increase almost linearly with time for the Gaussian, triangular and rectangular initial conditions considered in this study, and the largest and smallest wave temporal growth rates, i.e. the largest and the smallest values of s, correspond to the rectangular and triangular initial conditions, respectively, in accord with the results discussed in the previous section. The largest and the smallest values of s were found to be approximately equal to four-thousandths and three-thousandths, respectively, thus indicating that the solution temporal growth is slow.

Similar trends to the ones described in the previous paragraph have been found for $p = 2$ and $c^2 = 0.1$; however, for $p = 2$ and $c^2 = 10$, the values of $u_{\max}(t^*, x)$ for $\tau = 0.001, 0.01$ and 0.1 decrease with time, and the fastest decrease in wave amplitude has been found for the rectangular initial conditions, whereas the slowest one corresponds to the triangular ones. This is a consequence of the fact that, as stated above, for a fixed value of τ, the viscosity coefficient increases as c^2 is increased and, therefore, viscous effects and dissipation increase as c^2 is increased. On the other hand, the effect of viscosity decreases as c^2 is decreased and, therefore, the spatial gradient of the initial condition plays a key role on the initial dynamics of wave propagation for $c^2 \leq 1$ [cf. equations (6) and (8)].

The value of $u_{\max}(t^*, x)$ for $p = 3$ and $\tau = 0.001$ has been found to exhibit similar trends to the ones described above for $p = 2$ and $c^2 = 0.1$, i.e. it increases almost linearly with time for the three initial conditions considered here. On the other hand, for $p = 3$, $\tau = 0.01$ and $c^2 = 0.1, 1$ and 10, the values of $u_{\max}(t^*, x)$ have been found to increase almost exponentially with time, and the values of $|s|$ are about three times larger for $p = 3$ and $\tau = 0.001$ than for $p = 2$ and $c^2 = 0.1$. However, for $p = 3$, $\tau = 0.1$ and $c^2 = 10$, s has been found to be negative and have almost the same value for the three initial conditions considered in the paper.

From the numerical results used to obtain Table 2, it has been found that, for $c^2 = 0.1, 1$ and 10, $|s|$ decreases as c^2 is increased, is nearly independent of the initial conditions and is, at most, equal to one-thousandth and two percent for $p = 2$ and $\tau = 0.001$, and $p = 2$ and $\tau = 0.01$, respectively, thus indicating that $|s|$ increases as τ is increased, in agreement with the results reported previously, which show that the blowup time decreases as the relaxation time is increased.

For $\alpha = 1$, $p = 2$, $c^2 = 10$ and $\tau = 0.1$, it has been found that the values of $|s|$ for $A = 1.5$ are about 150% larger than those for $A = 1$, thus indicating that the solution temporal growth rate increases as the amplitude of the initial conditions and the effects of the nonlinear drift term are increased. $u_{\max}(t^*, x)$ has been found to be an almost linear function of time for $\tau = 0.001$ and $c^2 = 0.1, 1$ and 10 and an exponentially increasing (decreasing)

function of time for $\tau = 0.01$ ($\tau = 0.1$) and $c^2 = 0.1$, 1 and 10. This behavior is a consequence of the fact that the viscosity coefficient increases as either c^2 or τ is increased for fixed values of τ or c, respectively, and results in the curvature of the leading wave front location illustrated previously in Figures 1–20.

For $p = 3$ and $\tau = 0.01$, and the calculations performed to obtain the results illustrated in Table 2, it has been found that $|s|$ decreases as c^2 is increased and is larger for rectangular conditions than for triangular and Gaussian ones, and its largest value is approximately equal to four-thousandths. On the other hand, for $p = 3$, $c^2 = 10$ and $\tau = 0.001$, 0.01 and 0.1, it has been found that s is negative for Gaussian and triangular conditions and its magnitude increases as c^2 is increased. Moreover, it has also been found that, for $\tau = 0.001$ and 0.01, $u_{\max}(t^*, x)$ is an almost linearly increasing function of time, whereas for $\tau = 0.1$ is a decreasing function of time, for rectangular initial conditions.

From the results used to obtain Table 2 discussed in previous paragraphs as well as other ones not presented here, it may be stated that the value of $|s|$ increases as p and τ are increased for the three types of initial conditions analyzed in this study.

From the calculations carried out to obtain the results summarized in Table 3, $p = 2$, $c^2 = 10$ and $\tau = 0.001$, 0.01 and 0.1, the largest and smallest values of $|s|(s < 0)$ correspond to the rectangular and triangular conditions, respectively, and are about nine-thousandths and one-thousandth, respectively, thus indicating that the solution decay is very slow. These small values of $|s|$ are due to both the initial layer thickness whose duration in time is on the order of τ and the small value of μ; $|s|$ has been found to increase in magnitude as τ is increased, but its rate of increase decreases as the relaxation time is increased.

For $\tau = 0.001$ and 0.01, $u_{\max}(t^*, x)$ has been found to be an almost linear function of time, whereas it exhibits an exponential behavior for $\tau = 0.1$ on account of the increase of μ as τ is increased. The large values of $|s|$ observed for $c^2 = 10$ and rectangular conditions are a consequence of the fact that the slopes at the vertical sides of the rectangular conditions are Dirac delta functions, as stated in Section 2.3.

For $p = 2$, $\sigma = 0.1$, $\tau = 0.001$ and $c^2 = 0.1$, 1 and 10, rectangular initial conditions result in a larger value of $|s|$ than Gaussian ones, and the value of $|s|$ for the latter is larger than for triangular conditions, but the largest value of $|s|$ is approximately equal to one-thousandth. Similar trends have been observed, for $p = 3$, $\sigma = 0.1$, $\tau = 0.001$ and $c^2 = 0.1$, 1 and 10, but, in this case, the largest values of $|s|$ are about four times higher than those for $p = 2$ for Gaussian and rectangular initial conditions, whereas they are about twice those for $p = 2$ for triangular conditions, thus showing that the initial conditions for $p = 3$ play a much more important role in determining the temporal growth of the solution than for $p = 2$ in accord with the facts that the importance of the nonlinear advection term in equation (1) increases as p is increased and rectangular conditions are less smooth than triangular and Gaussian ones.

For $c^2 = 10$, $p = 3$ and $\tau = 0.001$, 0.01 and 0.1, it has been found that rectangular initial conditions result in larger values of $|s|$ than triangular ones, and the latter are characterized by larger values of $|s|$ than Gaussian ones. For the above parameters, s was found to be negative and exhibit a very strong exponential dependence on τ for $c^2 = 10$ and an almost linear one for $c^2 \le 1$. Similar trends to the ones just described have also been found for $p = 2$, $\sigma = 0.1$, $\tau = 0.01$ and $c^2 = 0.1$, 1 and 10. For these conditions, the values of s for $c^2 = 0.1$ and 1, and triangular conditions have been found to be at most 30% larger than those for Gaussian conditions, and the latter are about one-half those corresponding to rectangular conditions; the magnitude of $|s|$ for rectangular conditions is about 30% larger than those for Gaussian and triangular ones, for $c^2 = 10$.

For $p = 2$, $\tau = 0.01$, $\alpha = 0.1$, 1 and 2, and rectangular conditions, the numerical experiments performed to generate Table 4 result in larger values of $|s|$ than triangular ones, and the latter are, in turn, characterized by larger values of $|s|$ than Gaussian ones. For these values of the parameters, $|s|$ increases as α, i.e. the linear drift velocity, is increased, in accord with the steepening associated with the linear and nonlinear advection terms in equation (1) and the fact that the rectangular conditions are less smooth than the triangular ones, and the latter, in turn, are less smooth than the Gaussian conditions considered in this study. In addition, as shown in Figures 4 and 6 and Figures 18 and 20 for Gaussian and rectangular conditions, respectively, the speed of the leading wave front increases as α is increased.

By way of contrast, the results for $p = 2$ and $\tau = 0.001$ shown in Table 4 indicate that, for $\alpha = 0.1$, 1 and 2, the three initial conditions considered in the study reported here provide nearly the same value of s. But, although s increases as α is increased, its growth is much smaller than that observed for $\tau = 0.01$; this is a consequence of the fact that the thickness of the initial layer is proportional to τ and, therefore, decreases as τ is decreased. Note that the relaxation term in equation (1) is not present for $\tau = 0$.

For $p = 3$ and $\tau = 0.001$, similar results to the ones described above for $p = 2$ and $\tau = 0.001$ have been found, but $|s|$ is much larger for $p = 3$ than for $p = 2$, thus indicating once again the great importance of the nonlinear advection term on wave propagation.

4. Conclusions

An extensive numerical study of blowup of a one-dimensional, bidirectional nonlinear wave equation which becomes the well-known (inviscid) RLW or BBM equation and modified or generalized (inviscid) RLW equations when both the relaxation time and the viscosity coefficient are nil has been reported as a function of the parameters that appear in the equation and the amplitude and width of smooth and nonsmooth initial conditions. The smooth conditions are of the Gaussian type and are infinitely differentiable, whereas the nonsmooth ones are both piecewise-continuous and piecewise-differentiable.

The results of the numerical experiments indicate that, for an amplitude equal to unity, no blowup occurs for relaxation times less than or equal to one-hundredth, viscosity coefficients less than one-tenth, quadratic and cubic nonlinear advection terms, and Gaussian, triangular and rectangular initial conditions. No blowup has either been observed for the same relaxation times and viscosity coefficients as above, for quadratic nonlinearities and an amplitude equal to 1.5; however, for a cubic nonlinearity, relaxation times larger than one-hundredth and viscosity coefficients larger than one-tenth, blowup occurs for the three types of initial conditions considered in this study.

The blowup times for the triangular conditions have been found to be larger than those for the Gaussian ones, and the latter are larger than those for rectangular conditions, thus indicating that the blowup time decreases as the initial condition smoothness decreases and/or their slope increases. This finding is in accord with mathematical studies of the initial-value problem for the inviscid, three-dimensional Euler's equations.

The blowup time has also been found to decrease as the relaxation time, power of the nonlinearity, linear drift coefficient and amplitude of the initial conditions are increased, and as the width of the initial condition is decreased, but it increases as the viscosity coefficient is increased.

For a quadratic nonlinearity and a relaxation time and viscosity coefficient equal to one-tenth, the blowup time has been found to decrease by a factor of two when the linear drift coefficient was increased by a factor of twenty. On the other hand, for a cubic nonlinearity and the same relaxation time and viscosity coefficient, the blowup time decreases by less

than 34% as the linear drift velocity is increased. Moreover, for the same values of the linear drift coefficient and relaxation times, the blowup times for quadratic nonlinearities are about four times larger than those for cubic ones.

In some of the numerical experiments, it has been found that, depending on the linear drift coefficient, relaxation time, viscosity coefficient, degree of nonlinearity, and the shape, amplitude and width of the initial conditions, blowup does not occur for times less than the largest simulation time considered in this study. In such cases, a chord parameter based on the numerical solutions at two different times has been used to estimate the temporal growth/decay of the solution, and it has been found that the magnitude of the chord parameter increases as the nonsmoothness of the initial conditions is increased and is larger for the rectangular initial conditions than for the triangular ones. The chord parameter has also been found to increase as the power of the nonlinear drift, the linear advection coefficient, the relaxation time and the amplitude of the initial conditions are increased, but it decreases as the viscosity coefficient is increased.

It has also been found that the three initial conditions considered in this paper result in the formation of a leading wave front whose curvature depends on the parameters that characterize the one-dimensional, bidirectional equation as well as the initial conditions and that complex wave patterns appear between this leading wave and the upstream boundary. The number, amplitude and frequency of these waves have been found to increase as the nonsmoothness of the initial conditions is increased, in qualitative agreement with mathematical results for the three-dimensional, inviscid Euler's equation.

References

Banks, H.T., Giliam, D.S. and Shubov, V.I. (1997), "Global solvability for damped abstract nonlinear hyperbolic systems", *Differential and Integral Equations*, Vol. 10 No. 2, pp. 309-332.

Benjamin, T.B., Bona, J.L. and Mahony, J.J. (1972), "Model equations for long waves in nonlinear dispersive systems", *Philosophical Transactions of the Royal Society (London), Series A*, Vol. 272 No. 1220, pp. 47-78.

Bona, J.L., Chen, M. and Saut, J.-C. (2002), "Boussinesq equations and other systems for small-amplitude long waves in nonlinear dispersive media. I: derivation and linear theory", *Journal of Nonlinear Science*, Vol. 12 No. 4, pp. 283-318.

Bona, J.L., Chen, M. and Saut, J.-C. (2004), "Boussinesq equations and other systems for small-amplitude long waves in nonlinear dispersive media. II. The nonlinear theory", *Nonlinearity*, Vol. 17 No. 3, pp. 925-952.

Boussinesq, J. (1871), "Théorie de l'intumescence liquide, appelée onde solitaire ou de translation, se propageant dans un canal rectangulaire", *Comptes Rendus de L'Academie Des Sciences*, Vol. 72, pp. 755-759.

Boussinesq, J. (1872), "Théorie des ondes et des remous qui se propagent le long d'un canal rectangulaire horizontal, en communiquant au liquide contenu dans ce canal des vitesses sensiblement pareilles de la surface au fond", *Journal de Mathématiques Pures et Appliquées, Deuxième Série*, Vol. 17, pp. 55-108.

Burgers, J.M. (1948), "A mathematical model illustrating the theory of turbulence", von Mises, R. and von Karman, T. (Eds), *Advances in Applied Mechanics*, Eselvier, New York, Vol. 1, pp. 171-199.

Butuzov, V.F. (1997), "The angular boundary layer in mixed singularly perturbed problems for hyperbolic equations", *Mathematics of the USSR-Sbornik*, Vol. 33 No. 3, pp. 403-425.

Caffarelli, L.A. and Friedman, A. (1986), "The blow-up boundary for nonlinear wave equations", *Transactions of the American Mathematical Society*, Vol. 297 No. 1, pp. 223-241.

Carter, J.D. (2018), "Bidirectional Whitham equations as models of waves on shallow water", *Wave Motion*, Vol. 82, pp. 51-61.

Debnath, L. (1994), *Nonlinear Water Waves*, Academic Press, New York, NY.

Dingemans, M.W. (1997), *Water Wave Propagation over Uneven Bottoms*, Advanced Series on Ocean Engineering, Vol. 13 World Scientific, Singapore.

Dutykh, D. (2009), "Visco-potential free-surface flows and long wave modelling", *European Journal of Mechanics - B/Fluids*, Vol. 28 No. 3, pp. 430-443.

Dutykh, D. and Dias, F. (2007), "Dissipative Boussinesq equations", *Comptes Rendus Mécanique*, Vol. 335 Nos 9/10, pp. 559-583.

Elgindi, T.M. (2021), "Finite-time singularity formation for $C^{1,a}$ solutions to the incompressible Euler equations on $\mathbb{R}^3$", *Annals of Mathematics (2)*, Vol. 194 No. 3, pp. 647-727.

Escudero, C. (2007), "Blow-up of the hyperbolic Burgers equation", *Journal of Statistical Physics*, Vol. 127 No. 2, pp. 327-338.

García López, C.M. and Ramos, J.I. (2015), "Solitary waves generated by bell-shaped initial conditions in the inviscid and viscous GRLW equations", *Applied Mathematical Modelling*, Vol. 39 No. 21, pp. 6645-6668.

Johnson, R.S. (1997), *A Modern Introduction to the Mathematical Theory of Water Waves*, Cambridge University Press, New York, NY.

Joseph, D.D. and Preziosi, L. (1989), "Heat waves", *Review of Modern Physics*, Vol. 61 No. 1, pp. 41-73.

Joseph, D.D. and Preziosi, L. (1990), "Addendum to the paper 'heat waves'", *Review of Modern Physics*, Vol. 62 No. 2, pp. 375-391.

Jou, D., Pérez-García, C., García-Colín, L.S., López de Haro, M. and Rodríguez, R.F. (1985), "Generalized hydrodynamics and extended irreversible thermodynamics", *Physical Review A*, Vol. 31 No. 4, pp. 2502-2508.

Karakoç, S.B.G. and Zeybek, H. (2016), "Solitary-wave solutions of the GRLW equation using septic B-spline collocation method", *Applied Mathematics and Computation*, Vol. 289, pp. 159-171.

Karakoç, S.B.G., Ak, T. and Zeybek, H. (2014), "An efficient approach to numerical study of the MRLW equation with B-spline collocation method", *Abstract and Applied Analysis*, Vol. 2014 Article ID 596406.

Karakoç, S.B.G., Mei, L. and Ali, K.K. (2022), "Two efficient methods for solving the generalized regularized long wave equation", *Applicable Analysis*, Vol. 101 No. 13, pp. 4721-4742.

Karakoç, S.B.G., Uçar, Y. and YaÇ§murlu, N. (2015), "Numerical solutions of the MRLW equation by cubic B-spline Galerkin finite element method", *Kuwait Journal of Science*, Vol. 42 No. 2, pp. 141-159.

Karakoç, S.B.G., YaÇ§murlu, N.M. and Uç Ar, Y. (2013), "Numerical approximation to a solution of the modified regularized long wave equation using quintic B-splines", *Boundary Value Problems*, Vol. 2013 Article number 27.

Keener, J. and Sneyd, J. (2009), *Mathematical Physiology: II: Systems Physiology*, 2nd ed., Springer, New York, NY.

Kevorkian, J. and Cole, J.D. (1981), *Perturbation Methods in Applied Mathematics*, Springer-Verlag, New York, NY.

Kevorkian, J. and Cole, J.D. (1996), *Multiple Scale and Singular Perturbation Methods*, Springer, New York, NY.

Khonkin, A.D. (1980), "The paradox of the infinite velocity of travel of perturbations in hydrodynamics of viscous heat-conducting media, and equations of hydrodynamics of fast processes", *Fluid Mechanics-Soviet Research*, Vol. 9 No. 3, pp. 93-101.

Khonkin, A.D. and Orlov, A.V. (1993), "Weak shock structure on the basis of modified hydrodynamical equations", *Physics of Fluids A: Fluid Dynamics*, Vol. 5 No. 7, pp. 1810-1813.

Korteweg, D.J. and de Vries, G. (1895), "On the change of form of long waves advancing in a rectangular canal and on a new type of long stationary waves", *Philosophical Magazine, Series 5*, Vol. 39 No. 240, pp. 422-443.

Lannes, D. (2013), *The Water Waves Problem: Mathematical Analysis and Asymptotics*, American Mathematical Society, Providence, RI.

Le Meur, H.V. (2015), "Derivation of a viscous Boussinesq system for surface water waves", *Asymptotic Analysis*, Vol. 94 Nos 3/4, pp. 309-345.

Luo, G. and Hou, T.Y. (2014), "Potentially singular solutions of the 3D axisymmetric Euler equations", *Proceedings of the National Academy of Sciences (PNAS)*, Vol. 111 No. 36, pp. 12968-12973.

Luo, G. and Hou, T.Y. (2019), "Formation of finite-time singularities in the 3D axisymmetric Euler equations: a numerics guided study", *SIAM Review*, Vol. 61 No. 3, pp. 793-835.

McKean, H.P. (1981), "Boussinesq's equation on the circle", *Communications on Pure and Applied Mathematics*, Vol. 34 No. 5, pp. 599-691.

Mittal, R.C. and Dahiya, S. (2018), "A comparative study of modified cubic B-spline differential quadrature methods for a class of nonlinear viscous wave equations", *Engineering Computations*, Vol. 35 No. 1, pp. 315-333.

Mittal, R.C. and Rohila, R. (2018), "A fourth order cubic B-spline collocation method for the numerical study of the RLW and MRLW equations", *Wave Motion*, Vol. 80, pp. 47-68.

Onder, I., Cinar, M., Secer, A. and Bayram, M. (2023), "On soliton solutions of the modified equal width equation", *Engineering Computations*, Vol. 40 No. 5, pp. 1063-1083.

Peregrine, D.H. (1966), "Calculations of the development of an undular bore", *Journal of Fluid Mechanics*, Vol. 25 No. 2, pp. 321-330.

Peregrine, D.H. (1967), "Long waves on a beach", *Journal of Fluid Mechanics*, Vol. 27 No. 4, pp. 815-827.

Pierre, M. and Schmitt, D. (2000), "Blowup in reaction–diffusion systems with dissipation of mass", *SIAM Review*, Vol. 42 No. 1, pp. 93-106.

Ramos, J.I. (2006), "Explicit finite difference methods for the EW and RLW equations", *Applied Mathematics and Computation*, Vol. 179 No. 2, pp. 622-638.

Ramos, J.I. (2007), "Solitary waves of the EWE and RLW equations", *Chaos, Solitons and Fractals*, Vol. 34 No. 5, pp. 1498-1518.

Ramos, J.I. (2016), "On the accuracy of some explicit and implicit methods for the inviscid GRLW equation subject to initial Gaussian conditions", *International Journal of Numerical Methods for Heat and Fluid Flow*, Vol. 26Nos No. 3/4, pp. 698-721.

Ramos, J.I. and García López, C.M. (2017), "Time-linearized, compact methods for the inviscid GRLW equation subject to initial Gaussian conditions", *Applied Mathematical Modelling*, Vol. 48, pp. 353-383.

Ramos, J.I. and García López, C.M. (2020), "Effect of the initial conditions on a one-dimensional model of small-amplitude wave propagation in shallow water I: wave dynamics", *International Journal of Numerical Methods for Heat and Fluid Flow*, Vol. 30 No. 11, pp. 4979-5014.

Rinzel, J. and Keller, J.B. (1973), "Traveling wave solutions of a nerve conduction equation", *Biophysical Journal*, Vol. 13 No. 12, pp. 1313-1337.

Rosenau, P. (1993), "Random walker and the telegrapher's equation: a paradigm of a generalized hydrodynamics", *Physical Review E*, Vol. 48 No. 2, pp. R655-R657.

Saka, B., Şahin, A. and Dağ, I. (2011), "B-spline collocation algorithms for numerical solution of the RLW equation", *Numerical Methods for Partial Differential Equations*, Vol. 27 No. 3, pp. 581-607.

Whitham, G.B. (1974), *Linear and Nonlinear Water Waves*, John Wiley and Sons, New York, NY.

Wu, T.Y. (1994), "A bidirectional long-wave model", *Methods and Applications of Analysis*, Vol. 1 No. 1, pp. 108-117.

Yang, Z. and Wang, X. (2003), "Blowup of solutions for the 'bad' Boussinesq-type equation", *Journal of Mathematical Analysis and Applications*, Vol. 285 No. 1, pp. 282-298.

Yordanov, B. and Zhang, Q.S. (2005), "Finite-time blowup for wave equations with a potential", *SIAM Journal on Mathematical Analysis*, Vol. 36 No. 5, pp. 1426-1433.

Zhijian, Y. and Changming, S. (1997), "Blowup of solutions for a class of quasilinear evolution equations", *Nonlinear Analysis: Theory, Methods and Applications*, Vol. 28 No. 12, pp. 2017-2032.

Zeybek, H. and Karakoç, S.B.G. (2019), "A collocation algorithm based on quintic B-splines for the solitary wave simulation of the GRLW equation", *Scientia Iranica B*, Vol. 26 No. 6, pp. 3356-3368.

1226

Corresponding author
Carmen María García López can be contacted at: cmgl@lcc.uma.es